Comparative proteomics uncovers low asparagine content in Plasmodium tRip-KO proteins

Martina Pitolli, Marta Cela, Delphine Kapps, Johana Chicher, Laurence Despons, Magali Frugier

Comparative proteomics uncovers low asparagine content in *Plasmodium* tRip-KO proteins.

Martina Pitolli[1], Marta Cela[1#a], Delphine Kapps[1], Johana Chicher[2], Laurence Despons[1] and Magali Frugier[1*]

[1]Université de Strasbourg, CNRS, Architecture et Réactivité de l'ARN, UPR 9002, F-67084 Strasbourg, France

[2]Strasbourg-Esplanade Proteomics facility, Université de Strasbourg, F-67084 Strasbourg, France.

[#]Current address: Molecular Microbiology and Structural Biochemistry, CNRS UMR 5086, Université Claude Bernard Lyon 1, Lyon, France

*Corresponding author: m.frugier@ibmc-cnrs.unistra.fr

Abstract

tRNAs are not only essential for decoding the genetic code, but their abundance also has a strong impact on the rate of protein production, folding, and on the stability of the translated messenger RNAs. *Plasmodium* expresses a unique surface protein called tRip, involved in the import of exogenous tRNAs into the parasite. Comparative proteomic analysis of the blood stage of wild-type and tRip-KO variant of *P. berghei* parasites revealed that down-regulated proteins in the mutant parasite are distinguished by a bias in their asparagine content. Furthermore, the demonstration of the possibility of charging host tRNAs with *Plasmodium* aminoacyl-tRNA synthetases, led us to propose that, imported host tRNAs participate in parasite protein synthesis. These results also suggest a novel mechanism of translational control in which import of host tRNAs emerge as regulators of gene expression in the *Plasmodium* developmental cycle and pathogenesis, by enabling the synthesis of asparagine-rich regulatory proteins that efficiently and selectively control the parasite infectivity.

Introduction

We have discovered the only example to date of an exogenous tRNA import pathway, summarized in Fig. 1 [1–4]. In *Plasmodium*, the malaria parasite, *P. berghei* sporozoites (the extracellular infective form of the parasite, Supplementary Fig. S1a) isolated from the salivary glands of infected mosquitoes import exogenous tRNAs *via* a surface protein, named tRip (tRNA import protein). However, the absence of homologous mechanisms in other organisms raises the question of the role of this unique tRNA import and its mode of action. It has been established that (i) tRip is a homodimeric protein made of an N-terminal GST-like domain and a C-terminal EMAPII-like tRNA binding domain; (ii) tRip binds human tRNAs with high affinity *in vitro* and with a stoichiometry of one tRNA per tRip dimer; (iii) tRip is anchored to the parasite's plasma membrane with its tRNA binding domain exposed to the host system; (iv) immunolocalization experiments found tRip expressed both in the liver and blood stages in the vertebrate host, as well as in the intestine and salivary glands of the mosquito; (v) *in vitro*, exogenous tRNAs enter living sporozoites; (vi) the knockout parasite, tRip-KO, does not import tRNAs, its protein biosynthesis is significantly reduced, and its growth is decreased in vertebrate blood compared to the wild-type parasite.

Recently, the crystal structure of the dimeric N-terminal GST-like domain of *P. vivax* tRip was solved and revealed a unique homodimerization interface [5]. We confirmed by SAXS that this unusual interface exists in solution and that it allows Multi-Synthetase Complex (MSC) formation [3,4]. Indeed, tRip is an aminoacyl-tRNA synthetase interacting multifunctional protein (AIMP) since it specifically co-immunoprecipitate with three aminoacyl-tRNA synthetases (aaRS), namely glutamyl- (ERS), glutaminyl- (QRS) and methionyl- (MRS) tRNA synthetases; These aaRSs all contain an N-terminal GST-like domain involved in MSC assembly. Unexpectedly, these proteins form two exclusive heterotrimeric MSCs with a 2:2:2 stoichiometry: a Q-complex (tRip:ERS:QRS) and an M-complex (tRip:ERS:MRS) characterized by different biophysical properties and interaction networks (Fig. 1). We could also identify a set of host tRNAs preferentially bound by tRip (Fig. 1) and potentially best imported into the parasite. Interestingly, tRip does not bind to tRNAs in a sequence-dependent manner, but would rather recognize post-transcriptional modifications that modulate this interaction [2]. In contrast to what has been shown for its cytosolic homologue Arc1p in *Saccharomyces cerevisiae* [6], the tRNAs that best bind tRip do not match the aaRSs that compose MSCs. This suggests that, although tRip is an AIMP, it is not dedicated

to the aminoacylation of specific tRNAs (2), thereby leading us to search for a novel function for this unique membrane protein and the tRNA import with which it is associated.

The AIMP tRip is not the only protein that has been characterized as cytosolic in other organisms and is localized on the surface of *Plasmodium*. This is also the case for other RNA-binding proteins such as the poly-A binding protein-1 (PABP-1) [7] and the glyceraldehyde-3 phosphate dehydrogenase (GAPDH) [8], which are both found on the surface of the sporozoites. The presence of different RNA-binding proteins at the parasite-host interface is another indication that RNA exchange might control unsuspected host-parasite interactions that take place during the parasite life cycle. In the present study, we compared the proteomes of the wild-type (WT) and the tRip-KO blood stage parasites with the objective of understanding the fate of imported tRNAs in *Plasmodium* protein synthesis and its infectious process.

Results

Host tRNAs are aminoacylated by the cognate parasite aaRSs *in vitro*

Cross-aminoacylation reactions were tested using the aspartyl-, tyrosyl-, and asparaginyl-tRNA synthetases from *H. sapiens* and *P. falciparum* (Supplementary Fig. S2) *in vitro* to determine their ability to aminoacylate human $tRNA^{Asp}$, $tRNA^{Tyr}$, and $tRNA^{Asn}$, respectively using crude human tRNA (Fig. 2). These three aminoacylation systems are representative of the tRNAs recognized weakly (aspartate), moderately (tyrosine) and preferentially (asparagine) by tRip [2]. Aminoacylation plateaus show that all three *Plasmodium* aaRSs can aminoacylate nearly the same level of tRNA as their human counterparts, although asparaginylation by the parasite enzyme is effective on about 80% of human $tRNA^{Asn}$ isodecoders. It indicates that host tRNAs, when imported into parasites by tRip can be aminoacylated by parasite aaRSs to be used in protein translation.

Comparative proteomics of tRip-KO *versus* wild-type (WT) schizonts. We investigated the relative protein abundance of tRip-KO *versus* WT in the schizont stage of synchronized parasites (Supplementary Fig. S1b) using liquid chromatography coupled to tandem mass spectrometry (LC-MS/MS). To highlight the most relevant effects associated with the deletion of tRip, we chose to compare equal amounts of proteins, even though tRip-KO parasites grow slower than wild-type parasites and their translation efficiency is significantly reduced [1]. Three biological replicates for tRip-KO and WT were defined for the schizonts samples (Supplementary Dataset 1). The amounts of proteins (KO and

WT) were comparable as most proteins were stable in the proteomic data. This is notably the case for four constitutively highly expressed proteins: EF1-α (PBANKA_1133300), Hsp70 (PBANKA_0914400), enolase (PBANKA_1214300) and histone H4 (PBANKA_941900) (Supplementary Dataset 1). Protein abundance was calculated using the intensity of *P. berghei* peptides, which identified between 347 and 469 proteins. Metric multidimensional scaling (MDS) (included in Supplementary Dataset 1) indicated clustering of the tRip-KO and WT parasites, suggesting there are distinct groups of differentially abundant proteins between the two genotypes. Among these proteins, only 8 were significantly up-regulated and 49 were down-regulated in the tRip-KO parasites compared to the WT (*p-value* < 0.05) with a at least a 2-fold change in abundance; they are highlighted in the volcano plots in orange and green, respectively (Fig. 3a). Most of down-regulated proteins are involved in translation (31% ribosomal proteins, initiation, and elongation factors); the two other abundant categories were surface proteins involved in transport and invasion (16%) and proteins with unknown functions (14%) (Supplementary Dataset 1). Interestingly, the deregulated proteins include several aminoacyl-tRNA synthetases (aaRSs). The glutamyl-tRNA synthetase (ERS), which is tightly associated to tRip in the two plasmodium MSCs is reduced in the tRip-KO sample. However, the other two aaRSs associated with *Plasmodium* MSCs, i.e. glutaminyl- and methionyl-tRNA synthetases, are detected but their expression is not significantly affected. Moreover, both the lysyl- (KRS) and the asparaginyl (NRS) -tRNA synthetases are increased in the mutant compared to the WT parasite (Supplementary Dataset 1), NRS and ERS being just below the threshold with *p-values* of 0.0723 and 0.0627, respectively.

Amino acid compositions of tRip-KO down-regulated proteins in schizonts. Amino acid usage (percentage of amino acids) in the 100 most expressed stable proteins in the tRip-KO parasite was compared with that of the 49 significantly down-regulated proteins (Fig. 3b). There is no major increase in glutamate, methionine or glutamine usage in down-regulated proteins compared to the proteins efficiently expressed in the tRip-KO parasite, indicating that the dissociation of the two MSCs caused by tRip deletion does not directly affect protein synthesis in the mutant parasite. On the other hand, we clearly observe a 70% increase in asparagine in the proteins down-regulated in the tRip-KO parasite (Supplementary Dataset 2, 11.6% in downregulated proteins *versus* 6.8% stable proteins), thus, suggesting that the tRip-KO parasite has difficulty synthesizing asparagine-rich proteins. However, our analysis is global and our results do not mean that all down-regulated proteins in the tRip-KO parasite

are asparagine-rich. Only some of them are, but they are so rich in asparagine that they bias the content of the whole group.

Quantitative proteomics of tRip-KO *versus* WT in "blood stages" samples. Three biological replicates for tRip-KO and WT containing all blood stages (rings, trophozoites, and schizonts) were used for comparative proteomics (Supplementary Fig. S1b and Dataset 3). Triplicate proteomic data sets (KO and WT) were compared and identified between 617 and 1017 proteins each time. Sixty-nine proteins were significantly deregulated (at least a 2-fold change in abundance), 8 were up-regulated and 61 were down-regulated in the tRip-KO parasites compared to the WT (*p-value* < 0.05) (Fig. 3c). The few up-regulated proteins are especially rhoptry associated proteins (a specialized organelle in *Plasmodia*) and proteins involved in mobility and invasion (Supplementary Dataset 3), while down-regulated proteins were distributed across different functional families: Apart from the 20% of proteins with unknown function, most are involved in DNA replication (41%). Yet, none were common to the schizonts samples (compare Supplementary Data sets. S1 and S3). Amino acid usage in the tRip-KO down-regulated proteins shows also that these proteins contain more asparagine residues (10.5% at tRip-KO versus 7.8% at WT, i.e. 34% more) than the 150 most expressed stable proteins (Fig. 3d, and Supplementary Dataset 2), leading to the same conclusion as above: in the absence of tRip, asparagine-rich proteins are less efficiently synthesized.

The mRNAs encoding 3 down-regulated proteins (MCM7, ChAF1-C and one protein with unknown function) were quantified by qRT-PCR. They all showed a strong decrease in the tRip-KO parasite compared to the WT parasite (Supplementary Fig. S3b), suggesting that down-regulated proteins are controlled at the level of mRNA turnover (either transcription or degradation).

Identification of conserved asparagine-rich proteins in several *Plasmodia* species. Since both "schizonts" and "blood stages" samples strongly suggest that the tRip-KO parasite is hindered in inserting asparagine into proteins, the complete proteomes of six *Plasmodium* lineages (*P. falciparum*-5476 proteins, *P. berghei*-5076 proteins, *P. yoelii*-6097 proteins, *P. chabaudi*-5222 proteins, *P. knowlesi*-5340 proteins and *P. vivax*-6708 proteins) as well as *Toxoplasma gondii* (control, 8322 proteins) were retrieved from ApiDB [9] and analyzed for their asparagine content (Supplementary Fig. S4a). *Plasmodium* proteins contain more asparagine residues than *Toxoplasma*. Yet, the *P. knowlesi* and *P. vivax* proteomes contain fewer asparagine residues (about 8 %) than the 4 other *Plasmodia* strains (about 12%) (Supplementary Dataset 2 and Fig. S4a). Proteins were then ranked from highest

to lowest asparagine contents to identify those that might be impacted by decreased asparagine decoding efficiency. For all proteomes, only the top 0.5% proteins were considered to search for conserved proteins with the highest asparagine content. Depending on the strain, 25 to 30 proteins were selected (Fig. 4). Besides many proteins with unknown functions and different AP2 domain transcription factors, only 2 proteins are strictly conserved in all strains. They correspond to the CCR4-associated factor-1 (CAF-1) and the poly-A binding protein-3 (PABP-3). Both share the same ligand (poly-A sequence) and a peculiar modular organization. They feature a high-complexity N-terminal domain and a long low-complexity C-terminal domain containing a very large amount of asparagine residues (Supplementary Figs. S4b and S4c). The proportion of asparagine varies locally between 35 and 60% in *P. falciparum*, *P. yoelii*, *P. chabaudi* and *P. berghei* and between 20 and 25% in *P. knowlesi* and *P. vivax* (i.e. at least 3 times higher than their respective average usage of asparagine). Yet these two proteins are not detected or by only a few spectral counts in our proteomic data (Supplementary Data sets S1 and S3 in both WT and KO parasites).

Discussion

To achieve efficient and specific protein synthesis, codon usage of mRNA must be balanced with the availability of corresponding aminoacylated tRNAs in the cell (i.e.[10–13]). Any discrepancy can affect the rate of protein elongation in ribosomes and result in pauses in translation that lead to mRNA degradation [14]. It is interesting to note that blood contains reticulocytes, precursors of red blood cells (RBCs), which are very active in translation and therefore rich in tRNAs [15]. Both reticulocytes (about 2%) and mature RBC can be infected by *Plasmodia*. While reticulocytes are characterized by a dynamic protein synthesis, RBC are hyper-specialized anucleate cells that retain about 10 % of the protein synthesis observed in reticulocytes [16]. Despite their scarcity, *P. berghei* [17], *P.chabaudi* [18], *P. yoelii* [19] and *P. vivax* [20] have been shown to preferentially invade these tRNA-rich reticulocytes compared to mature RBCs.

Moreover, by comparing the proteomes of wild-type and tRip-KO *P. berghei*, we observed in two independent experiments that down-regulated proteins in the tRip-KO parasite are asparagine-rich proteins. Asparagine is the most used amino acid in the *P. berghei* proteome and is often found in long homorepeats [21,22]. This asparagine abundance is also found in *P. falciparum*, *P. chabaudi*, *P. yoelii* and to a lesser extent in *P.knowlesi* and *P. vivax* (Supplementary Fig. S4a), however proteins in the

latter two parasites do not contain long asparagine homorepeats. Based on these results, we propose that import of host $tRNA^{Asn}$ by tRip would ensure correct translation of asparagine-rich protein domains. In other words, the absence of tRNA import in the tRip-KO parasite would prevent the accumulation of host $tRNA^{Asn}$ and would thus explain why asparagine-rich proteins are poorly translated. This doesn't mean that two proteins with the same percentage of asparagine will necessarily be synthesized in the same way; the synthesis of a protein containing asparagine clusters will be reduced in the tRip-KO parasite, whereas the synthesis of a protein whose asparagines are evenly distributed in the sequence will be unaffected. This hypothesis is strongly supported by several observations: (i) asparaginyl- and lysyl-tRNA synthetases are overexpressed in the proteomes of tRip-KO schizonts (Fig. 3a, Supplementary Dataset 1). Both aaRSs aminoacylate tRNAs that are most used to synthesize *P. berghei* proteins. In general, increased expression of aminoacyl-tRNA synthetase correlates with a decrease in cognate aminoacyl-tRNA and/or amino acid [23,24]. This observation suggests, that $tRNA^{Asn}$ and $tRNA^{Lys}$ levels are low in tRip-KO schizonts. (ii) Furthermore, mammalian (human) $tRNA^{Asn}$ is among the tRNAs with the highest affinity for *P. falciparum* tRip, along with $tRNA^{Ser}_{AGA}$ and $tRNA^{Leu}_{hGA}$ (Fig. 1) [2]; It is reasonable to assume that the tRNAs with the highest affinity for tRip are also those that are most efficiently imported into the parasite. (iii) Finally, compensation for low $tRNA^{Asn}$ by tRip-mediated tRNA import is only possible if the host $tRNA^{Asn}$ is a substrate for the parasite AsnRS. This is indeed the case (Fig. 2) indicating that once in the parasite, at least some host $tRNA^{Asn}$ isoacceptors can be efficiently aminoacylated and used in parasite mRNA translation. We have previously shown that the *P. falciparum* AsnRS aminoacylates the human $tRNA^{Asn}$ transcript 8-fold less efficiently than its homologous *P. falciparum* transcript [38]. In contrast, in the present study, human $tRNA^{Asn}$ is efficiently charged by the *P. falciparum* enzyme, indicating that post-transcriptional modifications of human $tRNA^{Asn}$ are positively recognized by the parasite synthetase.

Two asparagine-rich proteins stand out and are conserved in the six *Plasmodium* species analyzed (Fig. 4): the CCr4-associated factor 1 (CAF-1), involved in the poly-(A) decay of mRNAs [25], and to the poly-(A) binding protein-3 (PABP3). Not only are both proteins involved in poly-(A) recognition, but they also adopt a common global structure with long asparagine-rich C-terminal domains found only in *Plasmodia* (Supplementary Figs. S4b and S4c). While PABP3 has not yet been characterized, CAF-1 has been studied in detail in *P. falciparum*. CAF-1 is an essential nuclease that degrades mRNAs enriched with non-optimally decoded codons. It belongs to the eukaryotic CCr4-Not complex, which

binds to the empty E-site of the ribosome and properly positions CAF-1 to initiate the decay of the 3′-poly(A)-tails of stalled mRNAs [26]. However, the asparagine-rich C-terminal domain of *P. falciparum* CAF-1 is not essential and it has been shown that its deletion leads to the premature release of non-infectious merozoites *in vitro* [27] and to the inappropriate development of gametocytes *in vivo* [28]. Interestingly, disruption of tRip and of the C-terminal domain of CAF-1 not only lead to the same phenotype: parasites have reduced infectivity and multiplication in the blood stage [1,27], but also results in overexpression of the same gene products involved in parasite egress and invasion: the rhoptry proteins, RAP1, RAP2/3 and the major surface proteins AMA-1 and MSP1 (Supplementary Dataset 3 and Fig. S4d). This suggests that tRip and CAF-1 may be linked in their cellular functions, i.e. in the tRip-KO parasite the absence of host $tRNA^{Asn}$ import would hinder the synthesis of the asparagine-rich C-terminus of CAF-1, and lead to the specific and premature expression of mRNAs encoding the proteins responsible for merozoite release and infectivity. Interestingly, this hypothesis is supported not only by the low level of tRip expression observed in this study at the schizont stage (compare tRip in Figs. 3a and 3c), but also by several transcriptomic datasets obtained on the individual blood stages of *P. berghei* and *P. falciparum* (https://plasmodb.org). Transcriptomes clearly show a significant reduction in tRip mRNA content in schizonts compared with ring and trophozoite stages. Thus, in the WT parasite, low tRip expression at the schizont stage could mimic what is proposed in this study for the tRip-KO parasite, i.e. lead to partial CAF-1 synthesis and timely release of mature merozoites from schizonts.

The complex life cycle of *Plasmodium* is highly regulated, involving tight transcriptional and especially post-transcriptional controls each time the parasite moves from one stage to another [29,30]. Translational regulation of specific proteins which depends on the availability of host tRNAs would enable efficient and rapid control of the transition from one stage to another during development. Failure to import host tRNAs could indicate to the parasite that the cell has run out of resources and that it's time to leave and infect another cell. In this respect, tissue-specific variations in tRNA levels and in their post-transcriptional modifications [31,32] represent diverse sources of tRNAs for import. Depending on the available tRNAs isodecoders, their concentration and their post-transcriptional modifications in the host cell, tRNA import could differentially control parasite translation and enable it to develop optimally not only in blood, but also in liver or mosquito. In this model, host tRNA supply could play a major role in parasite development by modulating the translation efficiency of certain mRNAs, while complying with the "just-in-time" translation model [29].

Methods

Ethic Statement: Experiments were carried out in conformity with the 2010/63/EU directive of the European regulation on the protection of animals used for scientific purposes. Our animal care facility received agreement #I-67-482-2 from the veterinary services of the département du Bas Rhin (Direction Départementale de la Protection des Populations). All experimental protocols including the animals was approved by the French ministry of higher education, research, and innovation under the agreements number APAFIS#11124-2018010312571506 v2. All experiments were performed in accordance with the ARRIVE guidelines.

Parasite production: Four- to six-week-old female mice (C57BL/6), weighing approximately 20 g, were injected intraperitoneally with 200 µL of frozen infected red blood cells (10-15% parasitemia diluted in phosphate-buffered saline (PBS)) either with wild-type (WT, *Pb* gfpGOMO14) or with tRip-KO (*Pb* tRip-KO mCherry) malaria parasites derived from the *P. berghei* (ANKA strain). Parasitemia was monitored daily by cytometry (BD Accuri C6). Mice with parasitemia between 5 and 10% were selected. Therefore, in this study, only mice without or low symptoms were used. These parasitemia levels were reached 3-6 days after parasite injection. Mice were put to sleep and blood was collected by intracardiac puncture (about 1 to 1.5 mL) and parasites were directly purified (all blood stages) or cultured for 24 hours in RPMI at 37°C under 5% CO2 (only schizonts) (Supplementary Fig. S1b) as described in [33].

infected blood was filtered through a Plasmodipur filter (Europroxima) to remove mouse leukocytes, centrifuged for 10 min at 450 g and recovered in 4 mL of RPMI. A 7.2 mL cushion of 60% isotonic Percoll was gently pipetted under the red blood cells and the tube was centrifuged for 20 min at 1450 g (swinging buckets), to separate infected red blood cells (iRBC) at the Percoll/RPMI interface from non-infected RBC at the bottom of the tube. Parasitized RBCs were recovered in 2 tubes, washed 3 times in 1 mL of PBS and combined with 200 µL each of PBS. Infected RBCs were then lysed with 0.02% saponin for 5 min in ice (in 400 µL). Free parasites were recovered by centrifugation for 5 min at 2000 g and washed in 500 µL of PBS. The two pellets were resuspended either in 50 µL of protein loading buffer and stored at -80°C until mass spectrometry analysis, or as is and placed at -80°C for RNA preparation.

Mass spectrometry (MS) and data analyses. Approximately 10 µg of protein was obtained from the half of the blood (~0.75 mL of a 5-10% infected mouse). Protein concentrations were determined by

Bradford assay using bovine serum albumin as the standard. Proteins were precipitated, reduced, and alkylated as described in [3]. After digestion overnight with sequencing grade porcine trypsin (300 ng, w/w, Promega, Fitchburg, MA, USA), the generated peptides were analyzed either using Easy-nanoLC-1000 system coupled to a Q-Exactive Plus mass spectrometer (Thermo Fisher Scientific, Germany) with 160-minutes gradients (blood stages) or a NanoLC-2DPlus system (nanoFlexChiP module; Eksigent, ABSciex, Concord, Ontario, Canada) coupled to a TripleTOF 5600 mass spectrometer (ABSciex) operating in positive mode with 120-minutes gradients (schizonts). Data were searched using the Mascot algorithm (version 2.6.2, Matrix Science) against the Uniprot database with *P.Berghei* taxonomy (release 2021_03, 4 927 sequences) with a decoy strategy. The resulting .dat Mascot files were then imported into Proline version 2.0 software [34] to align the identified proteins. Proteins were then validated with Mascot pretty rank equal to 1, and 1% false discovery rate (FDR) on both peptide spectrum matches (PSM) and protein sets (based on Mascot score). As expected for blood cells from infected mice, the number of contaminating mouse proteins represents between 40 and 50% of the proteins identified by mass spectrometry (Sup datasets 1 and 3).

For statistical analyses, raw Spectral Count values were imported into R (v. 3.5.0) where the number of spectra were first normalized using the DESeq2 median of ratio normalization method. A negative-binomial test using an edgeR GLM regression generated for each identified protein a p-value and a protein fold-change (FC). The R script used to process the dataset is published on Github [35]. Proteins were statistically enriched or decreased with a p-value < 0.05 and a minimum fold change (FC) of 2 or 0.5, respectively. Mass spectrometry proteomic data has been deposited within the ProteomeXchange Consortium via the PRIDE partner repository [36] with the dataset ID PXD043916 (**Username:** reviewer_pxd043916@ebi.ac.uk, **Password:** xu4rkrPE).

RNA purification and QRT-PCR. Total RNA was extracted from parasites using the RNeasy Mini Kit (Qiagen) according to the manufacturer's protocol and was subjected to DNAse treatment with the Rapid OUT DNA removal kit (Thermo Scientific). Total RNA was analyzed and quantified on Bioanalyser (puce PICO). Each sample was reverse transcribed in a 20 µL reaction volume containing 10 µL (0.16 to 0.5 µg) of RNA, using the SuperScript II reverse transcriptase (Invitrogen) according to the manufacturer's protocol. The mRNAs levels were measured by RT-PCR (25 µL containing 4 µL of cDNA) on a CFx94 (Bio-Rad) using the Syber Green kit (Thermo Scientific). Oligonucleotides used for qRT-PCR are listed in the Supplementary Fig. S3a. qRT-PCR reactions were designed according MIQE

guidelines [37], the specificity of the oligonucleotides was validated, and the amplification efficiencies of the primer sets are all between 90 and 110% and r^2 values greater than 0.96. The mRNAs levels were calculated according to the ΔCq method and normalized by the mRNA level of both the EF1-α and Hsp70 in each sample. Raw data are indicated as mean of three measurements, and results were expressed as the average of 3 biological samples ± standard error of the mean (SEM).

Purification of aminoacyl-tRNA synthetases and aminoacylation assays. Recombinant *P. falciparum* and *H. sapiens* NRS and DRS were cloned, expressed and purified as described in references [38,39] respectively. The gene encoding the *P. falciparum* TyrRS was amplified by PCR from *P. falciparum* cDNA and cloned into pQE30 (Qiagen) and the plasmid encoding the *H. sapiens* YRS was a gift from P. Schimmel. Both *P. falciparum* and *H. sapiens* YRS were expressed and purified as described for NRS [38]. Purified enzymes are shown in Supplementary Fig. S2. *H. sapiens* crude tRNAs was prepared as described in [2].

Aminoacylation assays were performed under the same conditions: at 37 °C for 2, 4 and 6 min in 50 mM HEPES-KOH (pH 7.5), 20 mM KCl, 10 mM $MgCl_2$, 2 mM ATP, 6 µM total tRNA from HeLa cells, in the presence of 20 µM of the corresponding L-[^{14}C]-amino acid (Perkin Elmer). AaRSs were diluted in 100 mM HEPES-KOH pH 7.5, 1 mM DTT, 5 mg/mL BSA, and 10% glycerol and used at a final concentration of 200 nM in the aminoacylation assay. The aminoacylation plateaus are the mean of 3 independent experiments ± standard deviation (SD).

Bioinformatics. Protein sequences as well as proteomes from all *Plasmodium* strains were retrieved from PlasmoDB. A home-made Python 2.7 script was used to calculate the asparagine content for each protein sequence. *Toxoplasma gondii* was the outgroup species.

References

[1] T. Bour, N. Mahmoudi, D. Kapps, S. Thiberge, D. Bargieri, R. Ménard, M. Frugier, *Apicomplexa*-specific tRip facilitates import of exogenous tRNAs into malaria parasites, Proc Natl Acad Sci USA 113 (2016) 4717–4722. https://doi.org/10.1073/pnas.1600476113.

[2] M. Cela, A. Théobald-Dietrich, J. Rudinger-Thirion, P. Wolff, R. Geslain, M. Frugier, Identification of host tRNAs preferentially recognized by the *Plasmodium* surface protein tRip, Nucleic Acids Research (2021) gkab769. https://doi.org/10.1093/nar/gkab769.

[3] J.R. Jaramillo Ponce, D. Kapps, C. Paulus, J. Chicher, M. Frugier, Discovery of two distinct aminoacyl-tRNA synthetase complexes anchored to the Plasmodium surface tRNA import protein, Journal of Biological Chemistry 298 (2022) 101987. https://doi.org/10.1016/j.jbc.2022.101987.

[4] J.R. Jaramillo Ponce, A. Théobald-Dietrich, P. Bénas, C. Paulus, C. Sauter, M. Frugier, Solution X-ray scattering highlights discrepancies in *Plasmodium* MULTI-AMINOACYL-TRNA synthetase complexes, Protein Science 32 (2023). https://doi.org/10.1002/pro.4564.

[5] S. Gupta, J. Chhibber-Goel, M. Sharma, S. Parvez, K. Harlos, A. Sharma, M. Yogavel, Crystal structures of the two domains that constitute the Plasmodium vivax p43 protein, Acta Crystallogr D Struct Biol 76 (2020) 135–146. https://doi.org/10.1107/S2059798319016413.

[6] K. Deinert, F. Fasiolo, E.C. Hurt, G. Simos, Arc1p Organizes the Yeast Aminoacyl-tRNA Synthetase Complex and Stabilizes Its Interaction with the Cognate tRNAs, Journal of Biological Chemistry 276 (2001) 6000–6008. https://doi.org/10.1074/jbc.M008682200.

[7] A.M. Minns, K.J. Hart, S. Subramanian, S. Hafenstein, S.E. Lindner, Nuclear, Cytosolic, and Surface-Localized Poly(A)-Binding Proteins of Plasmodium yoelii, mSphere 3 (2018). https://doi.org/10.1128/mSphere.00435-17.

[8] S.-J. Cha, M.-S. Kim, A. Pandey, M. Jacobs-Lorena, Identification of GAPDH on the surface of Plasmodium sporozoites as a new candidate for targeting malaria liver invasion, Journal of Experimental Medicine 213 (2016) 2099–2112. https://doi.org/10.1084/jem.20160059.

[9] C. Aurrecoechea, M. Heiges, H. Wang, Z. Wang, S. Fischer, P. Rhodes, J. Miller, E. Kraemer, C.J. Stoeckert, D.S. Roos, J.C. Kissinger, ApiDB: integrated resources for the apicomplexan bioinformatics resource center, Nucleic Acids Research 35 (2007) D427–D430. https://doi.org/10.1093/nar/gkl880.

[10] E.M. Novoa, L. Ribas de Pouplana, Speeding with control: codon usage, tRNAs, and ribosomes, Trends in Genetics 28 (2012) 574–581. https://doi.org/10.1016/j.tig.2012.07.006.

[11] J.D. Richter, J. Coller, Pausing on Polyribosomes: Make Way for Elongation in Translational Control, Cell 163 (2015) 292–300. https://doi.org/10.1016/j.cell.2015.09.041.

[12] M. Torrent, G. Chalancon, N.S. de Groot, A. Wuster, M. Madan Babu, Cells alter their tRNA abundance to selectively regulate protein synthesis during stress conditions, Sci. Signal. 11 (2018) eaat6409. https://doi.org/10.1126/scisignal.aat6409.

[13] P.C. Dedon, T.J. Begley, Dysfunctional tRNA reprogramming and codon-biased translation in cancer, Trends in Molecular Medicine 28 (2022) 964–978. https://doi.org/10.1016/j.molmed.2022.09.007.

[14] Q. Wu, S.G. Medina, G. Kushawah, M.L. DeVore, L.A. Castellano, J.M. Hand, M. Wright, A.A. Bazzini, Translation affects mRNA stability in a codon-dependent manner in human cells, eLife 8 (2019) e45396. https://doi.org/10.7554/eLife.45396.

[15] D.W.E. Smith, R.F. Randazzo, A.L. McNamara, The tRNA content of non-hemoglobinized red cell precursors: Evidence that tRNA content is controlled by tRNA utilization, Biochemical and Biophysical Research Communications 95 (1980) 468–473. https://doi.org/10.1016/0006-291X(80)90761-5.

[16] S.D. Kumar, D. Kar, M.N. Akhtar, B. Willard, D. Roy, T. Hussain, P.I. Rajyaguru, S.M. Eswarappa, Evidence for low-level translation in human erythrocytes, MBoC 33 (2022) br21. https://doi.org/10.1091/mbc.E21-09-0437.

[17] D. Cromer, K.J. Evans, L. Schofield, M.P. Davenport, Preferential invasion of reticulocytes during late-stage Plasmodium berghei infection accounts for reduced circulating reticulocyte levels, International Journal for Parasitology 36 (2006) 1389–1397. https://doi.org/10.1016/j.ijpara.2006.07.009.

[18] R. Antia, A. Yates, J.C. De Roode, The dynamics of acute malaria infections. I. Effect of the parasite's red blood cell preference, Proc. R. Soc. B. 275 (2008) 1449–1458. https://doi.org/10.1098/rspb.2008.0198.

[19] B. Mons, Preferential invasion of malarial merozoites into young red blood cells, Blood Cells 16 (1990) 299–312.

[20] N. Thawani, M. Tam, M.-J. Bellemare, D.S. Bohle, M. Olivier, J.B. De Souza, M.M. Stevenson, Plasmodium Products Contribute to Severe Malarial Anemia by Inhibiting Erythropoietin-Induced Proliferation of Erythroid Precursors, The Journal of Infectious Diseases 209 (2014) 140–149. https://doi.org/10.1093/infdis/jit417.

[21] S.R. Chaudhry, N. Lwin, D. Phelan, A.A. Escalante, F.U. Battistuzzi, Comparative analysis of low complexity regions in Plasmodia, Sci Rep 8 (2018) 335. https://doi.org/10.1038/s41598-017-18695-y.

[22] F.U. Battistuzzi, K.A. Schneider, M.K. Spencer, D. Fisher, S. Chaudhry, A.A. Escalante, Profiles of low complexity regions in Apicomplexa, BMC Evol Biol 16 (2016) 47. https://doi.org/10.1186/s12862-016-0625-0.

[23] Harald Putzer, Laalami Soumaya, Regulation of the Expression of Aminoacyl-tRNA Synthetases and Translation Factors, in: Madame Curie Bioscience Database, Landes Bioscience, 2000.

[24] O. Levi, S. Garin, Y. Arava, RNA mimicry in post-transcriptional regulation by aminoacyl tRNA synthetases, WIREs RNA 11 (2020). https://doi.org/10.1002/wrna.1564.

[25] M.A. Collart, The Ccr4-Not complex is a key regulator of eukaryotic gene expression, WIREs RNA 7 (2016) 438–454. https://doi.org/10.1002/wrna.1332.

[26] R. Buschauer, Y. Matsuo, T. Sugiyama, Y.-H. Chen, N. Alhusaini, T. Sweet, K. Ikeuchi, J. Cheng, Y. Matsuki, R. Nobuta, A. Gilmozzi, O. Berninghausen, P. Tesina, T. Becker, J. Coller, T. Inada, R. Beckmann, The Ccr4-Not complex monitors the translating ribosome for codon optimality, Science 368 (2020) eaay6912. https://doi.org/10.1126/science.aay6912.

[27] B. Balu, S.P. Maher, A. Pance, C. Chauhan, A.V. Naumov, R.M. Andrews, P.D. Ellis, S.M. Khan, J. Lin, C.J. Janse, J.C. Rayner, J.H. Adams, CCR4-Associated Factor 1 Coordinates the Expression of Plasmodium falciparum Egress and Invasion Proteins, Eukaryot Cell 10 (2011) 1257–1263. https://doi.org/10.1128/EC.05099-11.

[28] K.J. Hart, J. Oberstaller, M.P. Walker, A.M. Minns, M.F. Kennedy, I. Padykula, J.H. Adams, S.E. Lindner, Plasmodium male gametocyte development and transmission are critically regulated by the two putative deadenylases of the CAF1/CCR4/NOT complex, PLoS Pathog 15 (2019) e1007164. https://doi.org/10.1371/journal.ppat.1007164.

[29] S.S. Vembar, D. Droll, A. Scherf, Translational regulation in blood stages of the malaria parasite *Plasmodium spp.* : systems-wide studies pave the way: Translational regulation in blood stages of the malaria parasite, WIREs RNA 7 (2016) 772–792. https://doi.org/10.1002/wrna.1365.

[30] S. Bennink, G. Pradel, The molecular machinery of translational control in malaria parasites, Mol Microbiol 112 (2019) 1658–1673. https://doi.org/10.1111/mmi.14388.

[31] K.A. Dittmar, J.M. Goodenbour, T. Pan, Tissue-Specific Differences in Human Transfer RNA Expression, PLoS Genet 2 (2006) e221. https://doi.org/10.1371/journal.pgen.0020221.

[32] O. Pinkard, S. McFarland, T. Sweet, J. Coller, Quantitative tRNA-sequencing uncovers metazoan tissue-specific tRNA regulation, Nat Commun 11 (2020) 4104. https://doi.org/10.1038/s41467-020-17879-x.

[33] C. Ramakrishnan, M.J. Delves, K. Lal, A.M. Blagborough, G. Butcher, K.W. Baker, R.E. Sinden, Laboratory Maintenance of Rodent Malaria Parasites, in: R. Ménard (Ed.), Malaria, Humana Press, Totowa, NJ, 2012: pp. 51–72. https://doi.org/10.1007/978-1-62703-026-7_5.

[34] D. Bouyssié, A.-M. Hesse, E. Mouton-Barbosa, M. Rompais, C. Macron, C. Carapito, A. Gonzalez de Peredo, Y. Couté, V. Dupierris, A. Burel, J.-P. Menetrey, A. Kalaitzakis, J. Poisat, A. Romdhani, O. Burlet-Schiltz, S. Cianférani, J. Garin, C. Bruley, Proline: an efficient and user-friendly software suite for large-scale proteomics, Bioinformatics 36 (2020) 3148–3155. https://doi.org/10.1093/bioinformatics/btaa118.

[35] L. Kuhn, T. Vincent, P. Hammann, H. Zuber, Exploring Protein Interactome Data with IPinquiry: Statistical Analysis and Data Visualization by Spectral Counts, in: T. Burger (Ed.), Statistical Analysis of Proteomic Data, Springer US, New York, NY, 2023: pp. 243–265. https://doi.org/10.1007/978-1-0716-1967-4_11.

[36] Y. Perez-Riverol, J. Bai, C. Bandla, D. García-Seisdedos, S. Hewapathirana, S. Kamatchinathan, D.J. Kundu, A. Prakash, A. Frericks-Zipper, M. Eisenacher, M. Walzer, S. Wang, A. Brazma, J.A. Vizcaíno, The PRIDE database resources in 2022: a hub for mass spectrometry-based proteomics evidences, Nucleic Acids Research 50 (2022) D543–D552. https://doi.org/10.1093/nar/gkab1038.

[37] S.A. Bustin, V. Benes, J.A. Garson, J. Hellemans, J. Huggett, M. Kubista, R. Mueller, T. Nolan, M.W. Pfaffl, G.L. Shipley, J. Vandesompele, C.T. Wittwer, The MIQE Guidelines: Minimum Information for Publication of Quantitative Real-Time PCR Experiments, Clinical Chemistry 55 (2009) 611–622. https://doi.org/10.1373/clinchem.2008.112797.

[38] D. Filisetti, A. Théobald-Dietrich, N. Mahmoudi, J. Rudinger-Thirion, E. Candolfi, M. Frugier, Aminoacylation of Plasmodium falciparum tRNAAsn and Insights in the Synthesis of Asparagine Repeats, Journal of Biological Chemistry 288 (2013) 36361–36371. https://doi.org/10.1074/jbc.M113.522896.

[39] T. Bour, A. Akaddar, B. Lorber, S. Blais, C. Balg, E. Candolfi, M. Frugier, Plasmodial aspartyl-tRNA synthetases and peculiarities in Plasmodium falciparum, The Journal of Biological Chemistry 284 (2009) 18893–903.

[40] P.P. Chan, T.M. Lowe, GtRNAdb 2.0: an expanded database of transfer RNA genes identified in complete and draft genomes, Nucleic Acids Research 44 (2016) D184–D189. https://doi.org/10.1093/nar/gkv1309.

Aknowledgments

We are grateful to Philippe Hammann, Lauriane Kuhn, and Béatrice Chane Woon Ming for LC-MS/MS analysis, Fabrice Auge and Eric Marois for animal experiments, and to Dr Alain Lescure and Prof Tamara Hendrickson for providing comments on this manuscript.

This work was performed under the framework of the Interdisciplinary Thematic Institute IMCBio, as part of the ITI 2021-2028 program of the University of Strasbourg, CNRS and Inserm. It was supported by IdEx Unistra (ANR-10-IDEX-0002), by SFRI-STRAT'US project (ANR 20-SFRI-0012), and EUR IMCBio (IMCBio ANR-17-EURE-0023) under the framework of the French Investments for the Future Program », by previous Labex NetRNA (ANR-10-LABX-0036), by the CNRS and the Université de Strasbourg, IdEx "Equipement mi-lourd" (2015) and Equipement d'Excellence (EquipEx) I2MC (ANR-11-EQPX-0022), and by the Fondation pour la Recherche Médicale (FRM) (grant number FDT201704337050) to Marta Cela.

Authors Contributions

MP, DK and MC performed experiments, data acquisition, and analysis, JC performed mass spectrometry analysis and LD provided computer programming. MF managed the conception, design, interpretation of data and funding acquisition and wrote, reviewed, and edited the manuscript.

Data availability statement

All relevant data are within the manuscript and its Supporting Information files.

Additional information

Competing Interest Statement: The authors declare no conflict of interest.

1 pdf with 4 Supplementary Figures and 1 excel document containing 3 supplementary Data sets.

Figure legends

Figure 1. *P. berghei* membrane-bound multi-synthetase complexes. *Plasmodium* is characterized by the presence of two multisynthetase complexes (MSC) named Q-complex and M-complex. The Q-complex is composed of glutamyl- (ERS) and glutaminyl- (QRS) tRNA synthetases linked to a dimer of tRip whereas the M-complex is composed of tRip and Methionyl-tRNA synthetase (MRS) organized around a dimer of ERS. tRip is therefore an AIMP (Aminoacyl-tRNA synthetase Interacting Multifunctional Protein). tRip, ERS, QRS, and MRS are schematized and colored in grey, black, cyan, and orange, respectively. the GST-like domains are shown as a drop and the C-terminal domains of tRip, QRS and MRS involved in tRNA binding are either EMAPII-like domains (tRip and MRS, grey diamonds) or a positively charged α-helix (QRS, shown as a grey helix). The characteristic feature of *Plasmodium* MSCs is that tRip is a membrane protein (the transmembrane helix is shown in red) with the GST-like domain required for MSC formation localized inside the parasite and the tRNA binding domain exposed outside the parasite to host tRNAs. This unique organization justifies that only the EMAPII-like domain of tRip ($tRip_{200\text{-}402}$) is fused at the C-terminal domain of a GST domain and used as a target for the selection of aptamers capable of inhibiting tRip tRNA binding. Interfaces 1, 1' or 2, involved in protein-protein interactions, are indicated in the corresponding GST-like domains. For the sake of simplicity, this illustration does not show the parasitophorous membrane that surrounds the parasite in the infected red blood cell.

Figure 2. Cross aminoacylation of host tRNAs by the parasite aminoacyl-tRNA synthetases. Six aaRSs, aspartyl-, asparaginyl- and tyrosyl-tRNA synthetases from *H. sapiens* (in blue) or *P. falciparum* (in orange) were tested with crude human tRNAs under the same experimental conditions (6 µM crude tRNA and 0.2 µM aaRSs). Aminoacylation plateaus were measured at 6 min of incubation. Human crude tRNAs are potentially transcribed from 420 genes, amongst which 19 genes encode $tRNA^{Asp}$, 34 genes encoding $tRNA^{Asn}$ and 15 genes encoding $tRNA^{Tyr}$ [40]. Error bars represent the standard deviation (SEM) of three independent experiments.

Figure 3. Comparative proteomic analysis and amino acid usage of proteins identified in WT and tRip-KO samples containing schizonts (a and b) or all blood stages (c and d). (**a**) Volcano plot of all quantified proteins from WT and tRip-KO parasites displaying the relationship between statistical significance (−log10(*p-value*), y-axis) and log fold change (FC) of each protein (log2(FC), x-axis). Statistics are based on three independent experiments (Supplementary Dataset 1). Deregulated

proteins in tRip-KO parasite compared to the WT parasite are shown in orange (up-regulated, FC≥2 and *p-value* ≤ 0.05) and green (down-regulated, FC≤-1 and *p-value* ≤ 0.05). tRip is shown in red and black dots represent proteins with no significant change. ERS, KRS and NRS correspond to glutamyl-, lysyl- and asparaginyl-tRNA synthetases; ERS and NRS are shown as black circles surrounded by grenn and orange, respectively because their *p-values* are slightly greater than 0.05. (**b**) Comparison of amino acid usage (%) of proteins whose expression is stable in the tRip-KO parasite (the 100 most expressed proteins, black) and all proteins that are down-regulated in the tRip-KO parasite (green). Amino acids are designated by their one letter symbol and the total number of amino acids used in the analyses is specified. (**c**) Volcano plot of all quantified proteins from WT and tRip-KO parasites. Statistics are based on three independent experiments (Supplementary Dataset 3). (**d**) Comparison of amino acid usage (%) between proteins whose expression is stable in the tRip-KO parasite (the 150 most expressed proteins, black) and proteins down-regulated in the tRip-KO parasite (green).

Figure 4. Top 0.5% of the most asparagine-rich proteins in 6 *Plasmodium* strains. Six *Plasmodium* species were selected: *P. falciparum*, *P. yoelii*, *P. berghei*, *P. chabaudi*, all featuring high asparagine usage (around 12%, Supplementary Fig. S4a) often localized in homorepetitions and *P. knowlesi* and *P. vivax* which show lower asparagine usage (around 8%, Supplementary Fig. S4a) and no homorepeats. Proteins highlighted in yellow are proteins of unknown function, light green indicate AP2 family regulatory proteins and dark green show the two proteins conserved in all 6 species, regardless of their asparagine usage.

Introduction

We have discovered the only example to date of an exogenous tRNA import pathway, summarized in Fig. 1 [1–4]. In *Plasmodium*, the malaria parasite, *P. berghei* sporozoites (the extracellular infective form of the parasite, Supplementary Fig. S1a) isolated from the salivary glands of infected mosquitoes import exogenous tRNAs *via* a surface protein, named tRip (tRNA import protein). However, the absence of homologous mechanisms in other organisms raises the question of the role of this unique tRNA import and its mode of action. It has been established that (i) tRip is a homodimeric protein made of an N-terminal GST-like domain and a C-terminal EMAPII-like tRNA binding domain; (ii) tRip binds human tRNAs with high affinity *in vitro* and with a stoichiometry of one tRNA per tRip dimer; (iii) tRip is anchored to the parasite's plasma membrane with its tRNA binding domain exposed to the host system; (iv) immunolocalization experiments found tRip expressed both in the liver and blood stages in the vertebrate host, as well as in the intestine and salivary glands of the mosquito; (v) *in vitro*, exogenous tRNAs enter living sporozoites; (vi) the knockout parasite, tRip-KO, does not import tRNAs, its protein biosynthesis is significantly reduced, and its growth is decreased in vertebrate blood compared to the wild-type parasite.

Recently, the crystal structure of the dimeric N-terminal GST-like domain of *P. vivax* tRip was solved and revealed a unique homodimerization interface [5]. We confirmed by SAXS that this unusual interface exists in solution and that it allows Multi-Synthetase Complex (MSC) formation [3,4]. Indeed, tRip is an aminoacyl-tRNA synthetase interacting multifunctional protein (AIMP) since it specifically co-immunoprecipitate with three aminoacyl-tRNA synthetases (aaRS), namely glutamyl- (ERS), glutaminyl- (QRS) and methionyl- (MRS) tRNA synthetases; These aaRSs all contain an N-terminal GST-like domain involved in MSC assembly. Unexpectedly, these proteins form two exclusive heterotrimeric MSCs with a 2:2:2 stoichiometry: a Q-complex (tRip:ERS:QRS) and an M-complex (tRip:ERS:MRS) characterized by different biophysical properties and interaction networks (Fig. 1). We could also identify a set of host tRNAs preferentially bound by tRip (Fig. 1) and potentially best imported into the parasite. Interestingly, tRip does not bind to tRNAs in a sequence-dependent manner, but would rather recognize post-transcriptional modifications that modulate this interaction [2]. In contrast to what has been shown for its cytosolic homologue Arc1p in *Saccharomyces cerevisiae* [6], the tRNAs that best bind tRip do not match the aaRSs that compose MSCs. It suggests that, although tRip is an AIMP, it is not dedicated to

the aminoacylation of specific tRNAs (2), thereby leading us to search for a novel function for this unique membrane protein and the tRNA import with which it is associated.

The AIMP tRip is not the only protein that has been characterized as cytosolic in other organisms and is localized on the surface of *Plasmodium*. This is also the case for other RNA-binding proteins such as the poly-A binding protein-1 (PABP-1) [7] and the glyceraldehyde-3 phosphate dehydrogenase (GAPDH) [8], which are both found on the surface of the sporozoites. The presence of different RNA-binding proteins at the parasite-host interface is another indication that RNA exchange might control unsuspected host-parasite interactions that take place during the parasite life cycle. In the present study, we compared the proteomes of the wild-type (WT) and the tRip-KO blood stage parasites with the objective of understanding the fate of imported tRNAs in *Plasmodium* protein synthesis and its infectious process.

Results

Host tRNAs are aminoacylated by the cognate parasite aaRSs *in vitro*

Cross-aminoacylation reactions were tested using the aspartyl-, tyrosyl-, and asparaginyl-tRNA synthetases from *H. sapiens* and *P. falciparum* (Supplementary Fig. S2) *in vitro* to determine their ability to aminoacylate human $tRNA^{Asp}$, $tRNA^{Tyr}$, and $tRNA^{Asn}$, respectively using crude human tRNA (Fig. 2). These three aminoacylation systems are representative of the tRNAs recognized weakly (aspartate), moderately (tyrosine) and preferentially (asparagine) by tRip [2]. Aminoacylation plateaus show that all three *Plasmodium* aaRSs can aminoacylate nearly the same level of tRNA as their human counterparts, although asparaginylation by the parasite enzyme is effective on about 80% of human $tRNA^{Asn}$ isodecoders. It indicates that host tRNAs, when imported into parasites by tRip can be aminoacylated by parasite aaRSs to be used in protein translation.

Comparative proteomics of tRip-KO *versus* wild-type (WT) schizonts. We investigated the relative protein abundance of tRip-KO *versus* WT in the schizont stage of synchronized parasites (Supplementary Fig. S1b) using liquid chromatography coupled to tandem mass spectrometry (LC-MS/MS). To highlight the most relevant effects associated with the deletion of tRip, we chose to compare equal amounts of proteins, even though tRip-KO parasites grow slower than wild-type parasites and their translation efficiency is significantly reduced [1]. Three biological replicates for tRip-KO and WT were defined for the schizonts samples (Supplementary Dataset 1). The amounts of proteins (KO and

WT) were comparable as most proteins were stable in the proteomic data. This is notably the case for four constitutively highly expressed proteins: EF1-α (PBANKA_1133300), Hsp70 (PBANKA_0914400), enolase (PBANKA_1214300) and histone H4 (PBANKA_941900) (Supplementary Dataset 1). Protein abundance was calculated using the intensity of *P. berghei* peptides, which identified between 347 and 469 proteins. Metric multidimensional scaling (MDS) (included in Supplementary Dataset 1) indicated clustering of the tRip-KO and WT parasites, suggesting there are distinct groups of differentially abundant proteins between the two genotypes. Among these proteins, only 8 were significantly up-regulated and 49 were down-regulated in the tRip-KO parasites compared to the WT (*p-value* < 0.05) with a at least a 2-fold change in abundance; they are highlighted in the volcano plots in orange and green, respectively (Fig. 3a). Most of down-regulated proteins are involved in translation (31% ribosomal proteins, initiation, and elongation factors); the two other abundant categories were surface proteins involved in transport and invasion (16%) and proteins with unknown functions (14%) (Supplementary Dataset 1). Interestingly, the deregulated proteins include several aminoacyl-tRNA synthetases. The glutamyl-tRNA synthetase (ERS), which is tightly associated to tRip in the two plasmodium MSCs is reduced in the tRip-KO sample and both the lysyl- (KRS) and the asparaginyl (NRS) -tRNA synthetases are increased in the mutant compared to the WT parasite (Supplementary Dataset 1), NRS and ERS being just below the threshold with *p-values* of 0.0723 and 0.0627, respectively.

Amino acid compositions of tRip-KO down-regulated proteins in schizonts. Amino acid usage (percentage of amino acids) in the 100 most expressed stable proteins in the tRip-KO parasite was compared with that of the 49 significantly down-regulated proteins (Fig. 3b). There is no major increase in glutamate, methionine or glutamine usage in down-regulated proteins compared to the proteins efficiently expressed in the tRip-KO parasite, indicating that the dissociation of the two MSCs caused by tRip deletion does not directly affect protein synthesis in the mutant parasite. On the other hand, we clearly observe a 70% increase in asparagine in the proteins down-regulated in the tRip-KO parasite (Supplementary Dataset 2, 11.6% in downregulated proteins *versus* 6.8% stable proteins), thus, suggesting that the tRip-KO parasite has difficulty synthesizing asparagine-rich proteins.

Quantitative proteomics of tRip-KO *versus* WT in "blood stages" samples. Three biological replicates for tRip-KO and WT containing all blood stages (rings, trophozoites, and schizonts) were used for comparative proteomics (Supplementary Fig. S1b and Dataset 3). Triplicate proteomic data sets (KO and WT) were compared and identified between 617 and 1017 proteins each time. Sixty-nine proteins

were significantly deregulated (at least a 2-fold change in abundance), 8 were up-regulated and 61 were down-regulated in the tRip-KO parasites compared to the WT (*p-value* < 0.05) (Fig. 3c). The few up-regulated proteins are especially rhoptry associated proteins (a specialized organelle in *Plasmodia*) and proteins involved in mobility and invasion (Supplementary Dataset 3), while down-regulated proteins were distributed across different functional families: Apart from the 20% of proteins with unknown function, most are involved in DNA replication (41%). Yet, none were common to the schizonts samples (compare Supplementary Data sets. S1 and S3). Amino acid usage in the tRip-KO down-regulated proteins shows also that these proteins contain more asparagine residues (10.5% at tRip-KO versus 7.8% at WT, i.e. 34% more) than the 150 most expressed stable proteins (Fig. 3d, and Supplementary Dataset 2), leading to the same conclusion as above: in the absence of tRip, asparagine-rich proteins are less efficiently synthesized.

The mRNAs encoding 3 down-regulated proteins (MCM7, ChAF1-C and one protein with unknown function) were quantified by qRT-PCR. They all showed a strong decrease in the tRip-KO parasite compared to the WT parasite (Supplementary Fig. S3b), suggesting that down-regulated proteins are controlled at the level of mRNA turnover.

Identification of conserved asparagine-rich proteins in several *Plasmodia* strains. Since both "schizonts" and “blood stages” samples strongly suggest that the tRip-KO parasite is hindered in inserting asparagine into proteins, the complete proteomes of six *Plasmodium* lineages (*P. falciparum*-5476 proteins, *P. berghei*-5076 proteins, *P. yoelii*-6097 proteins, *P. chabaudi*-5222 proteins, *P. knowlesi*-5340 proteins and *P. vivax*-6708 proteins) as well as *Toxoplasma gondii* (control, 8322 proteins) were retrieved from ApiDB [9] and analyzed for their asparagine content (Supplementary Fig. S4a). *Plasmodium* proteins contain more asparagine residues than *Toxoplasma*. Yet, the *P. knowlesi* and *P. vivax* proteomes contain fewer asparagine residues (about 8 %) than the 4 other *Plasmodia* strains (about 12%) (Supplementary Dataset 2 and Fig. S4a). Proteins were then ranked from highest to lowest asparagine contents to identify those that might be impacted by decreased asparagine decoding efficiency. For all proteomes, only the top 0.5% proteins were considered to search for conserved proteins with the highest asparagine content. Depending on the strain, 25 to 30 proteins were selected (Fig. 4). Besides many proteins with unknown functions and different AP2 domain transcription factors, only 2 proteins are strictly conserved in all strains. They correspond to the CCR4-associated factor-1 (CAF-1) and the poly-A binding protein-3 (PABP-3). Both share the same ligand (poly-A

sequence) and a peculiar modular organization. They feature a high-complexity N-terminal domain and a long low-complexity C-terminal domain containing a very large amount of asparagine residues (Supplementary Figs. S4b and S4c). The proportion of asparagine varies locally between 35 and 60% in *P. falciparum*, *P. yoelii*, *P. chabaudi* and *P. berghei* and between 20 and 25% in *P. knowlesi* and *P. vivax* (i.e. at least 3 times higher than their respective average usage of asparagine). Yet these two proteins are not detected or by only a few spectral counts in our proteomic data (Supplementary Data sets S1 and S3).

Discussion

To achieve efficient and specific protein synthesis, codon usage of mRNA must be balanced with the availability of corresponding aminoacylated tRNAs in the cell (i.e.[10–13]). Any discrepancy can affect the rate of protein elongation in ribosomes and result in pauses in translation that lead to mRNA degradation [14]. It is interesting to note that blood contains reticulocytes, precursors of RBCs, which are very active in translation and therefore rich in tRNAs [15]. Both reticulocytes (about 2%) and mature red blood cells (RBC) can be infected by *Plasmodia*. While reticulocytes are characterized by a dynamic protein synthesis, RBC are hyper-specialized anucleate cells that retain about 10 % of the protein synthesis observed in reticulocytes [16]. Despite their scarcity, *P. berghei* [17], *P.chabaudi* [18], *P. yoelii* [19] and *P. vivax* [20] have been shown to preferentially invade these tRNA-rich reticulocytes compared to mature RBCs.

Moreover, by comparing the proteomes of wild-type and tRip-KO *P. berghei*, we observed in two independent experiments that down-regulated proteins in the tRip-KO parasite are asparagine-rich proteins. Asparagine is the most used amino acid in the *P. berghei* proteome and is often found in long homorepeats [21,22]. This asparagine abundance is also found in *P. falciparum*, *P. chabaudi*, *P. yoelii* and to a lesser extent in *P.knowlesi* and *P. vivax* (Supplementary Fig. S4a), however proteins in the latter two parasites do not contain long asparagine repeats. Based on these results, we propose that import of host $tRNA^{Asn}$ by tRip would ensure correct translation of asparagine-rich protein domains. In other words, the absence of tRNA import in the tRip-KO parasite would prevent the accumulation of host $tRNA^{Asn}$ and would thus explain why asparagine-rich proteins are poorly translated. This hypothesis is strongly supported by several observations: (i) asparaginyl- and lysyl-tRNA synthetases are overexpressed in the proteomes of tRip-KO schizonts (Fig. 3a, Supplementary Dataset 1). Both aaRSs

aminoacylate tRNAs that are most used to synthesize *P. berghei* proteins. In general, increased expression of aminoacyl-tRNA synthetase correlates with a decrease in cognate aminoacyl-tRNA and/or amino acid [23,24]. This observation suggests, that $tRNA^{Asn}$ and $tRNA^{Lys}$ levels are low in tRip-KO schizonts. (ii) Furthermore, mammalian (human) $tRNA^{Asn}$ is among the tRNAs with the highest affinity for *P. falciparum* tRip, along with $tRNA^{Ser}_{AGA}$ and $tRNA^{Leu}_{hGA}$ (Fig. 1) [2]; It is reasonable to assume that the tRNAs with the highest affinity for tRip are also those that are most efficiently imported into the parasite. (iii) Finally, compensation for low $tRNA^{Asn}$ by tRip-mediated tRNA import is only possible if the host $tRNA^{Asn}$ is a substrate for the parasite AsnRS. This is indeed the case (Fig. 2) indicating that once in the parasite, at least some host $tRNA^{Asn}$ isoacceptors can be efficiently aminoacylated and used in parasite mRNA translation. We have previously shown that the *P. falciparum* AsnRS aminoacylates the human $tRNA^{Asn}$ transcript 8-fold less efficiently than its homologous *P. falciparum* transcript [38]. In contrast, in the present study, human $tRNA^{Asn}$ is efficiently charged by the *P. falciparum* enzyme, indicating that post-transcriptional modifications of human $tRNA^{Asn}$ are positively recognized by the parasite synthetase.

Two asparagine-rich proteins stand out and are conserved in the six *Plasmodium* species analyzed (Fig. 4): the CCr4-associated factor 1 (CAF-1), involved in the poly-(A) decay of mRNAs [25], and to the poly-(A) binding protein-3 (PABP3). Not only are both proteins involved in poly-(A) recognition, but they also adopt a common global structure with long asparagine-rich C-terminal domains found only in *Plasmodia* (Supplementary Figs. S4b and S4c). While PABP3 has not yet been characterized, CAF-1 has been studied in detail in *P. falciparum*. CAF-1 is an essential nuclease that degrades mRNAs enriched with non-optimally decoded codons. It belongs to the eukaryotic CCr4-Not complex, which binds to the empty E-site of the ribosome and properly positions CAF-1 to initiate the decay of the 3′-poly(A)-tails of stalled mRNAs [26]. However, the asparagine-rich C-terminal domain of *P. falciprum* CAF-1 is not essential and it has been shown that its deletion leads to the premature release of non-infectious merozoites *in vitro* [27] and to the inappropriate development of gametocytes *in vivo* [28]. Interestingly, disruption of tRip and of the C-terminal domain of CAF-1 not only lead to the same phenotype: parasites have reduced infectivity and multiplication in the blood stage [1,27], but also results in overexpression of the same gene products involved in parasite egress and invasion: the rhoptry proteins, RAP1, RAP2/3 and the major surface proteins AMA-1 and MSP1 (Supplementary Dataset 3 and Fig. S4d). It suggests that tRip and CAF-1 may be linked in their cellular functions, i.e. in the tRip-

KO parasite the absence of host $tRNA^{Asn}$ import would hinder the synthesis of the asparagine-rich C-terminus of CAF-1, and lead to the specific and premature expression of mRNAs encoding the proteins responsible for merozoite release and infectivity.

The complex life cycle of *Plasmodium* is highly regulated, involving tight transcriptional and especially post-transcriptional controls each time the parasite moves from one stage to another [29,30]. Translational regulation of specific proteins which depends on the availability of host tRNAs would enable efficient and rapid control of the transition from one stage to another during development. Failure to import host tRNAs could indicate to the parasite that the cell has run out of resources and that it's time to leave and infect another cell. In this respect, tissue-specific variations in tRNA levels and in their post-transcriptional modifications [31,32] represent diverse sources of tRNAs for import. Depending on the available tRNAs isodecoders, their concentration and their post-transcriptional modifications in the host cell, tRNA import could differentially control parasite translation and enable it to develop optimally not only in blood, but also in liver or mosquito. In this model, host tRNA supply could play a major role in parasite development by modulating the translation efficiency of certain mRNAs, while complying with the "just-in-time" translation model [29].

Methods

Ethic Statement: Experiments were carried out in conformity with the 2010/63/EU directive of the European regulation on the protection of animals used for scientific purposes. Our animal care facility received agreement #I-67-482-2 from the veterinary services of the département du Bas Rhin (Direction Départementale de la Protection des Populations). All experimental protocols including the animals was approved by the French ministry of higher education, research, and innovation under the agreements number APAFIS#11124-2018010312571506 v2. All experiments were performed in accordance with the ARRIVE guidelines.

Parasite production: Four- to six-week-old female mice (C57BL/6), weighing approximately 20 g, were injected intraperitoneally with 200 µL of frozen infected red blood cells (10-15% parasitemia diluted in phosphate-buffered saline (PBS)) either with wild-type (WT, *Pb* gfpGOMO14) or with tRip-KO (*Pb* tRip-KO mCherry) malaria parasites derived from the *P. berghei* (ANKA strain). Parasitemia was monitored daily by cytometry (BD Accuri C6). Mice with parasitemia between 5 and 10% were selected. Therefore, in this study, only mice without or low symptoms were used. These parasitemia levels were

reached 3-6 days after parasite injection. Mice were put to sleep and blood was collected by intracardiac puncture (about 1 to 1.5 mL) and parasites were directly purified (all blood stages) or cultured for 24 hours in RPMI at 37°C under 5% CO2 (only schizonts) (Supplementary Fig. S1b) as described in [33].

infected blood was filtered through a Plasmodipur filter (Europroxima) to remove mouse leukocytes, centrifuged for 10 min at 450 g and recovered in 4 mL of RPMI. A 7.2 mL cushion of 60% isotonic Percoll was gently pipetted under the red blood cells and the tube was centrifuged for 20 min at 1450 g (swinging buckets), to separate infected red blood cells (iRBC) at the Percoll/RPMI interface from non-infected RBC at the bottom of the tube. Parasitized RBCs were recovered in 2 tubes, washed 3 times in 1 mL of PBS and combined with 200 µL each of PBS. Infected RBCs were then lysed with 0.02% saponin for 5 min in ice (in 400 µL). Free parasites were recovered by centrifugation for 5 min at 2000 g and washed in 500 µL of PBS. The two pellets were resuspended either in 50 µL of protein loading buffer and stored at -80°C until mass spectrometry analysis, or as is and placed at -80°C for RNA preparation.

Mass spectrometry (MS) and data analyses. Approximately 10 µg of protein was obtained from the half of the blood (~0.75 mL of a 5-10% infected mouse). Protein concentrations were determined by Bradford assay using bovine serum albumin as the standard. Proteins were precipitated, reduced, and alkylated as described in [3]. After digestion overnight with sequencing grade porcine trypsin (300 ng, w/w, Promega, Fitchburg, MA, USA), the generated peptides were analyzed either using Easy-nanoLC-1000 system coupled to a Q-Exactive Plus mass spectrometer (Thermo Fisher Scientific, Germany) with 160-minutes gradients (blood stages) or a NanoLC-2DPlus system (nanoFlexChiP module; Eksigent, ABSciex, Concord, Ontario, Canada) coupled to a TripleTOF 5600 mass spectrometer (ABSciex) operating in positive mode with 120-minutes gradients (schizonts). Data were searched using the Mascot algorithm (version 2.6.2, Matrix Science) against the Uniprot database with *P.Berghei* taxonomy (release 2021_03, 4 927 sequences) with a decoy strategy. The resulting .dat Mascot files were then imported into Proline version 2.0 software [34] to align the identified proteins. Proteins were then validated with Mascot pretty rank equal to 1, and 1% false discovery rate (FDR) on both peptide spectrum matches (PSM) and protein sets (based on Mascot score). As expected for blood cells from infected mice, the number of contaminating mouse proteins represents between 40 and 50% of the proteins identified by mass spectrometry (Sup datasets 1 and 3).

For statistical analyses, raw Spectral Count values were imported into R (v. 3.5.0) where the number of spectra were first normalized using the DESeq2 median of ratio normalization method. A negative-binomial test using an edgeR GLM regression generated for each identified protein a p-value and a protein fold-change (FC). The R script used to process the dataset is published on Github [35]. Proteins were statistically enriched or decreased with a p-value < 0.05 and a minimum fold change (FC) of 2 or 0.5, respectively. Mass spectrometry proteomic data has been deposited within the ProteomeXchange Consortium via the PRIDE partner repository [36] with the dataset ID PXD043916 (**Username:** reviewer_pxd043916@ebi.ac.uk, **Password:** xu4rkrPE).

RNA purification and QRT-PCR. Total RNA was extracted from parasites using the RNeasy Mini Kit (Qiagen) according to the manufacturer's protocol and was subjected to DNAse treatment with the Rapid OUT DNA removal kit (Thermo Scientific). Total RNA was analyzed and quantified on Bioanalyser (puce PICO). Each sample was reverse transcribed in a 20 µL reaction volume containing 10 µL (0.16 to 0.5 µg) of RNA, using the SuperScript II reverse transcriptase (Invitrogen) according to the manufacturer's protocol. The mRNAs levels were measured by RT-PCR (25 µL containing 4 µL of cDNA) on a CFx94 (Bio-Rad) using the Syber Green kit (Thermo Scientific). Oligonucleotides used for qRT-PCR are listed in the Supplementary Fig. S3a. qRT-PCR reactions were designed according MIQE guidelines [37], the specificity of the oligonucleotides was validated, and the amplification efficiencies of the primer sets are all between 90 and 110% and r^2 values greater than 0.96. The mRNAs levels were calculated according to the ΔCq method and normalized by the mRNA level of both the EF1-α and Hsp70 in each sample. Raw data are indicated as mean of three measurements, and results were expressed as the average of 3 biological samples ± standard error of the mean (SEM).

Purification of aminoacyl-tRNA synthetases and aminoacylation assays. Recombinant *P. falciparum* and *H. sapiens* NRS and DRS were cloned, expressed and purified as described in references [38,39] respectively. The gene encoding the *P. falciparum* TyrRS was amplified by PCR from *P. falciparum* cDNA and cloned into pQE30 (Qiagen) and the plasmid encoding the *H. sapiens* YRS was a gift from P. Schimmel. Both *P. falciparum* and *H. sapiens* YRS were expressed and purified as described for NRS [38]. Purified enzymes are shown in Supplementary Fig. S2. *H. sapiens* crude tRNAs was prepared as described in [2].

Aminoacylation assays were performed under the same conditions: at 37 °C for 2, 4 and 6 min in 50 mM HEPES-KOH (pH 7.5), 20 mM KCl, 10 mM $MgCl_2$, 2 mM ATP, 6 µM total tRNA from HeLa cells,

in the presence of 20 µM of the corresponding L-[^{14}C]-amino acid (Perkin Elmer). AaRSs were diluted in 100 mM HEPES-KOH pH 7.5, 1 mM DTT, 5 mg/mL BSA, and 10% glycerol and used at a final concentration of 200 nM in the aminoacylation assay. The aminoacylation plateaus are the mean of 3 independent experiments ± standard deviation (SD).

Bioinformatics. Protein sequences as well as proteomes from all *Plasmodium* strains were retrieved from PlasmoDB. A home-made Python 2.7 script was used to calculate the asparagine content for each protein sequence. *Toxoplasma gondii* was the outgroup species.

References

[1] T. Bour, N. Mahmoudi, D. Kapps, S. Thiberge, D. Bargieri, R. Ménard, M. Frugier, *Apicomplexa*-specific tRip facilitates import of exogenous tRNAs into malaria parasites, Proc Natl Acad Sci USA 113 (2016) 4717–4722. https://doi.org/10.1073/pnas.1600476113.

[2] M. Cela, A. Théobald-Dietrich, J. Rudinger-Thirion, P. Wolff, R. Geslain, M. Frugier, Identification of host tRNAs preferentially recognized by the *Plasmodium* surface protein tRip, Nucleic Acids Research (2021) gkab769. https://doi.org/10.1093/nar/gkab769.

[3] J.R. Jaramillo Ponce, D. Kapps, C. Paulus, J. Chicher, M. Frugier, Discovery of two distinct aminoacyl-tRNA synthetase complexes anchored to the Plasmodium surface tRNA import protein, Journal of Biological Chemistry 298 (2022) 101987. https://doi.org/10.1016/j.jbc.2022.101987.

[4] J.R. Jaramillo Ponce, A. Théobald-Dietrich, P. Bénas, C. Paulus, C. Sauter, M. Frugier, Solution X-ray scattering highlights discrepancies in *Plasmodium* MULTI-AMINOACYL-tRNA synthetase complexes, Protein Science 32 (2023). https://doi.org/10.1002/pro.4564.

[5] S. Gupta, J. Chhibber-Goel, M. Sharma, S. Parvez, K. Harlos, A. Sharma, M. Yogavel, Crystal structures of the two domains that constitute the Plasmodium vivax p43 protein, Acta Crystallogr D Struct Biol 76 (2020) 135–146. https://doi.org/10.1107/S2059798319016413.

[6] K. Deinert, F. Fasiolo, E.C. Hurt, G. Simos, Arc1p Organizes the Yeast Aminoacyl-tRNA Synthetase Complex and Stabilizes Its Interaction with the Cognate tRNAs, Journal of Biological Chemistry 276 (2001) 6000–6008. https://doi.org/10.1074/jbc.M008682200.

[7] A.M. Minns, K.J. Hart, S. Subramanian, S. Hafenstein, S.E. Lindner, Nuclear, Cytosolic, and Surface-Localized Poly(A)-Binding Proteins of Plasmodium yoelii, mSphere 3 (2018). https://doi.org/10.1128/mSphere.00435-17.

[8] S.-J. Cha, M.-S. Kim, A. Pandey, M. Jacobs-Lorena, Identification of GAPDH on the surface of Plasmodium sporozoites as a new candidate for targeting malaria liver invasion, Journal of Experimental Medicine 213 (2016) 2099–2112. https://doi.org/10.1084/jem.20160059.

[9] C. Aurrecoechea, M. Heiges, H. Wang, Z. Wang, S. Fischer, P. Rhodes, J. Miller, E. Kraemer, C.J. Stoeckert, D.S. Roos, J.C. Kissinger, ApiDB: integrated resources for the apicomplexan bioinformatics resource center, Nucleic Acids Research 35 (2007) D427–D430. https://doi.org/10.1093/nar/gkl880.

[10] E.M. Novoa, L. Ribas de Pouplana, Speeding with control: codon usage, tRNAs, and ribosomes, Trends in Genetics 28 (2012) 574–581. https://doi.org/10.1016/j.tig.2012.07.006.

[11] J.D. Richter, J. Coller, Pausing on Polyribosomes: Make Way for Elongation in Translational Control, Cell 163 (2015) 292–300. https://doi.org/10.1016/j.cell.2015.09.041.

[12] M. Torrent, G. Chalancon, N.S. de Groot, A. Wuster, M. Madan Babu, Cells alter their tRNA abundance to selectively regulate protein synthesis during stress conditions, Sci. Signal. 11 (2018) eaat6409. https://doi.org/10.1126/scisignal.aat6409.

[13] P.C. Dedon, T.J. Begley, Dysfunctional tRNA reprogramming and codon-biased translation in cancer, Trends in Molecular Medicine 28 (2022) 964–978. https://doi.org/10.1016/j.molmed.2022.09.007.

[14] Q. Wu, S.G. Medina, G. Kushawah, M.L. DeVore, L.A. Castellano, J.M. Hand, M. Wright, A.A. Bazzini, Translation affects mRNA stability in a codon-dependent manner in human cells, eLife 8 (2019) e45396. https://doi.org/10.7554/eLife.45396.

[15] D.W.E. Smith, R.F. Randazzo, A.L. McNamara, The tRNA content of non-hemoglobinized red cell precursors: Evidence that tRNA content is controlled by tRNA utilization, Biochemical and Biophysical Research Communications 95 (1980) 468–473. https://doi.org/10.1016/0006-291X(80)90761-5.

[16] S.D. Kumar, D. Kar, M.N. Akhtar, B. Willard, D. Roy, T. Hussain, P.I. Rajyaguru, S.M. Eswarappa, Evidence for low-level translation in human erythrocytes, MBoC 33 (2022) br21. https://doi.org/10.1091/mbc.E21-09-0437.

[17] D. Cromer, K.J. Evans, L. Schofield, M.P. Davenport, Preferential invasion of reticulocytes during late-stage Plasmodium berghei infection accounts for reduced circulating reticulocyte levels,

International Journal for Parasitology 36 (2006) 1389–1397. https://doi.org/10.1016/j.ijpara.2006.07.009.

[18] R. Antia, A. Yates, J.C. De Roode, The dynamics of acute malaria infections. I. Effect of the parasite's red blood cell preference, Proc. R. Soc. B. 275 (2008) 1449–1458. https://doi.org/10.1098/rspb.2008.0198.

[19] B. Mons, Preferential invasion of malarial merozoites into young red blood cells, Blood Cells 16 (1990) 299–312.

[20] N. Thawani, M. Tam, M.-J. Bellemare, D.S. Bohle, M. Olivier, J.B. De Souza, M.M. Stevenson, Plasmodium Products Contribute to Severe Malarial Anemia by Inhibiting Erythropoietin-Induced Proliferation of Erythroid Precursors, The Journal of Infectious Diseases 209 (2014) 140–149. https://doi.org/10.1093/infdis/jit417.

[21] S.R. Chaudhry, N. Lwin, D. Phelan, A.A. Escalante, F.U. Battistuzzi, Comparative analysis of low complexity regions in Plasmodia, Sci Rep 8 (2018) 335. https://doi.org/10.1038/s41598-017-18695-y.

[22] F.U. Battistuzzi, K.A. Schneider, M.K. Spencer, D. Fisher, S. Chaudhry, A.A. Escalante, Profiles of low complexity regions in Apicomplexa, BMC Evol Biol 16 (2016) 47. https://doi.org/10.1186/s12862-016-0625-0.

[23] Harald Putzer, Laalami Soumaya, Regulation of the Expression of Aminoacyl-tRNA Synthetases and Translation Factors, in: Madame Curie Bioscience Database, Landes Bioscience, 2000.

[24] O. Levi, S. Garin, Y. Arava, RNA mimicry in post-transcriptional regulation by aminoacyl tRNA synthetases, WIREs RNA 11 (2020). https://doi.org/10.1002/wrna.1564.

[25] M.A. Collart, The Ccr4-Not complex is a key regulator of eukaryotic gene expression, WIREs RNA 7 (2016) 438–454. https://doi.org/10.1002/wrna.1332.

[26] R. Buschauer, Y. Matsuo, T. Sugiyama, Y.-H. Chen, N. Alhusaini, T. Sweet, K. Ikeuchi, J. Cheng, Y. Matsuki, R. Nobuta, A. Gilmozzi, O. Berninghausen, P. Tesina, T. Becker, J. Coller, T. Inada, R. Beckmann, The Ccr4-Not complex monitors the translating ribosome for codon optimality, Science 368 (2020) eaay6912. https://doi.org/10.1126/science.aay6912.

[27] B. Balu, S.P. Maher, A. Pance, C. Chauhan, A.V. Naumov, R.M. Andrews, P.D. Ellis, S.M. Khan, J. Lin, C.J. Janse, J.C. Rayner, J.H. Adams, CCR4-Associated Factor 1 Coordinates the

Expression of Plasmodium falciparum Egress and Invasion Proteins, Eukaryot Cell 10 (2011) 1257–1263. https://doi.org/10.1128/EC.05099-11.

[28] K.J. Hart, J. Oberstaller, M.P. Walker, A.M. Minns, M.F. Kennedy, I. Padykula, J.H. Adams, S.E. Lindner, Plasmodium male gametocyte development and transmission are critically regulated by the two putative deadenylases of the CAF1/CCR4/NOT complex, PLoS Pathog 15 (2019) e1007164. https://doi.org/10.1371/journal.ppat.1007164.

[29] S.S. Vembar, D. Droll, A. Scherf, Translational regulation in blood stages of the malaria parasite *Plasmodium spp.* : systems-wide studies pave the way: Translational regulation in blood stages of the malaria parasite, WIREs RNA 7 (2016) 772–792. https://doi.org/10.1002/wrna.1365.

[30] S. Bennink, G. Pradel, The molecular machinery of translational control in malaria parasites, Mol Microbiol 112 (2019) 1658–1673. https://doi.org/10.1111/mmi.14388.

[31] K.A. Dittmar, J.M. Goodenbour, T. Pan, Tissue-Specific Differences in Human Transfer RNA Expression, PLoS Genet 2 (2006) e221. https://doi.org/10.1371/journal.pgen.0020221.

[32] O. Pinkard, S. McFarland, T. Sweet, J. Coller, Quantitative tRNA-sequencing uncovers metazoan tissue-specific tRNA regulation, Nat Commun 11 (2020) 4104. https://doi.org/10.1038/s41467-020-17879-x.

[33] C. Ramakrishnan, M.J. Delves, K. Lal, A.M. Blagborough, G. Butcher, K.W. Baker, R.E. Sinden, Laboratory Maintenance of Rodent Malaria Parasites, in: R. Ménard (Ed.), Malaria, Humana Press, Totowa, NJ, 2012: pp. 51–72. https://doi.org/10.1007/978-1-62703-026-7_5.

[34] D. Bouyssié, A.-M. Hesse, E. Mouton-Barbosa, M. Rompais, C. Macron, C. Carapito, A. Gonzalez de Peredo, Y. Couté, V. Dupierris, A. Burel, J.-P. Menetrey, A. Kalaitzakis, J. Poisat, A. Romdhani, O. Burlet-Schiltz, S. Cianférani, J. Garin, C. Bruley, Proline: an efficient and user-friendly software suite for large-scale proteomics, Bioinformatics 36 (2020) 3148–3155. https://doi.org/10.1093/bioinformatics/btaa118.

[35] L. Kuhn, T. Vincent, P. Hammann, H. Zuber, Exploring Protein Interactome Data with IPinquiry: Statistical Analysis and Data Visualization by Spectral Counts, in: T. Burger (Ed.), Statistical Analysis of Proteomic Data, Springer US, New York, NY, 2023: pp. 243–265. https://doi.org/10.1007/978-1-0716-1967-4_11.

[36] Y. Perez-Riverol, J. Bai, C. Bandla, D. García-Seisdedos, S. Hewapathirana, S. Kamatchinathan, D.J. Kundu, A. Prakash, A. Frericks-Zipper, M. Eisenacher, M. Walzer, S. Wang, A. Brazma, J.A.

Vizcaíno, The PRIDE database resources in 2022: a hub for mass spectrometry-based proteomics evidences, Nucleic Acids Research 50 (2022) D543–D552. https://doi.org/10.1093/nar/gkab1038.

[37] S.A. Bustin, V. Benes, J.A. Garson, J. Hellemans, J. Huggett, M. Kubista, R. Mueller, T. Nolan, M.W. Pfaffl, G.L. Shipley, J. Vandesompele, C.T. Wittwer, The MIQE Guidelines: Minimum Information for Publication of Quantitative Real-Time PCR Experiments, Clinical Chemistry 55 (2009) 611–622. https://doi.org/10.1373/clinchem.2008.112797.

[38] D. Filisetti, A. Théobald-Dietrich, N. Mahmoudi, J. Rudinger-Thirion, E. Candolfi, M. Frugier, Aminoacylation of Plasmodium falciparum tRNAAsn and Insights in the Synthesis of Asparagine Repeats, Journal of Biological Chemistry 288 (2013) 36361–36371. https://doi.org/10.1074/jbc.M113.522896.

[39] T. Bour, A. Akaddar, B. Lorber, S. Blais, C. Balg, E. Candolfi, M. Frugier, Plasmodial aspartyl-tRNA synthetases and peculiarities in Plasmodium falciparum, The Journal of Biological Chemistry 284 (2009) 18893–903.

[40] P.P. Chan, T.M. Lowe, GtRNAdb 2.0: an expanded database of transfer RNA genes identified in complete and draft genomes, Nucleic Acids Research 44 (2016) D184–D189. https://doi.org/10.1093/nar/gkv1309.

Aknowledgments

We are grateful to Philippe Hammann, Lauriane Kuhn, and Béatrice Chane Woon Ming for LC-MS/MS analysis, Fabrice Auge and Eric Marois for animal experiments, and to Dr Alain Lescure and Prof Tamara Hendrickson for providing comments on this manuscript.

This work was performed under the framework of the Interdisciplinary Thematic Institute IMCBio, as part of the ITI 2021-2028 program of the University of Strasbourg, CNRS and Inserm. It was supported by IdEx Unistra (ANR-10-IDEX-0002), by SFRI-STRAT'US project (ANR 20-SFRI-0012), and EUR IMCBio (IMCBio ANR-17-EURE-0023) under the framework of the French Investments for the Future Program », by previous Labex NetRNA (ANR-10-LABX-0036), by the CNRS and the Université de Strasbourg, IdEx "Equipement mi-lourd" (2015) and Equipement d'Excellence (EquipEx) I2MC (ANR-11-EQPX-0022), and by the Fondation pour la Recherche Médicale (FRM) (grant number FDT201704337050) to Marta Cela.

Authors Contributions

MP, DK and MC performed experiments, data acquisition, and analysis, JC performed mass spectrometry analysis and LD provided computer programming. MF managed the conception, design, interpretation of data and funding acquisition and wrote, reviewed, and edited the manuscript.

Data availability statement

All relevant data are within the manuscript and its Supporting Information files.

Additional information

Competing Interest Statement: The authors declare no conflict of interest.

1 pdf with 4 Supplementary Figures and 1 excel document containing 3 supplementary Data sets.

Figure legends

Figure 1. *P. berghei* membrane-bound multi-synthetase complexes. *Plasmodium* is characterized by the presence of two multisynthetase complexes (MSC) named Q-complex and M-complex. The Q-complex is composed of glutamyl- (ERS) and glutaminyl- (QRS) tRNA synthetases linked to a dimer of tRip whereas the M-complex is composed of tRip and Methionyl-tRNA synthetase (MRS) organized around a dimer of ERS. tRip is therefore an AIMP (Aminoacyl-tRNA synthetase Interacting Multifunctional Protein). tRip, ERS, QRS, and MRS are schematized and colored in grey, black, cyan, and orange, respectively. the GST-like domains are shown as a drop and the C-terminal domains of tRip, QRS and MRS involved in tRNA binding are either EMAPII-like domains (tRip and MRS, grey diamonds) or a positively charged α-helix (QRS, shown as a grey helix). The characteristic feature of *Plasmodium* MSCs is that tRip is a membrane protein (the transmembrane helix is shown in red) with the GST-like domain required for MSC formation localized inside the parasite and the tRNA binding domain exposed outside the parasite to host tRNAs. This unique organization justifies that only the EMAPII-like domain of tRip ($tRip_{200\text{-}402}$) is fused at the C-terminal domain of a GST domain and used as a target for the selection of aptamers capable of inhibiting tRip tRNA binding. Interfaces 1, 1' or 2, involved in protein-protein interactions, are indicated in the corresponding GST-like domains. For the sake of simplicity, this illustration does not show the parasitophorous membrane that surrounds the parasite in the infected red blood cell.

Figure 2. Cross aminoacylation of host tRNAs by the parasite aminoacyl-tRNA synthetases. Six aaRSs, aspartyl-, asparaginyl- and tyrosyl-tRNA synthetases from *H. sapiens* (in blue) or *P. falciparum* (in orange) were tested with crude human tRNAs under the same experimental conditions (6 µM crude tRNA and 0.2 µM aaRSs). Aminoacylation plateaus were measured at 6 min of incubation. Human crude tRNAs are potentially transcribed from 420 genes, amongst which 19 genes encode $tRNA^{Asp}$, 34 genes encoding $tRNA^{Asn}$ and 15 genes encoding $tRNA^{Tyr}$ [40]. Error bars represent the standard deviation (SEM) of three independent experiments.

Figure 3. Comparative proteomic analysis and amino acid usage of proteins identified in WT and tRip-KO samples containing schizonts (a and b) or all blood stages (c and d). (**a**) Volcano plot of all quantified proteins from WT and tRip-KO parasites displaying the relationship between statistical significance (−log10(*p-value*), y-axis) and log fold change (FC) of each protein (log2(FC), x-axis). Statistics are based on three independent experiments (Supplementary Dataset 1). Deregulated

proteins in tRip-KO parasite compared to the WT parasite are shown in orange (up-regulated, FC≥2 and *p-value* ≤ 0.05) and green (down-regulated, FC≤-1 and *p-value* ≤ 0.05). tRip is shown in red and black dots represent proteins with no significant change. ERS, KRS and NRS correspond to glutamyl-, lysyl- and asparaginyl-tRNA synthetases; ERS and NRS are shown as black circles surrounded by grenn and orange, respectively because their *p-values* are slightly greater than 0.05. (**b**) Comparison of amino acid usage (%) of proteins whose expression is stable in the tRip-KO parasite (the 100 most expressed proteins, black) and all proteins that are down-regulated in the tRip-KO parasite (green). Amino acids are designated by their one letter symbol and the total number of amino acids used in the analyses is specified. (**c**) Volcano plot of all quantified proteins from WT and tRip-KO parasites. Statistics are based on three independent experiments (Supplementary Dataset 3). (**d**) Comparison of amino acid usage (%) between proteins whose expression is stable in the tRip-KO parasite (the 150 most expressed proteins, black) and proteins down-regulated in the tRip-KO parasite (green).

Figure 4. Top 0.5% of the most asparagine-rich proteins in 6 *Plasmodium* strains. Six *Plasmodium* species were selected: *P. falciparum*, *P. yoelii*, *P. berghei*, *P. chabaudi*, all featuring high asparagine usage (around 12%, Supplementary Fig. S4a) often localized in homorepetitions and *P. knowlesi* and *P. vivax* which show lower asparagine usage (around 8%, Supplementary Fig. S4a) and no homorepeats. Proteins highlighted in yellow are proteins of unknown function, light green indicate AP2 family regulatory proteins and dark green show the two proteins conserved in all 6 species, regardless of their asparagine usage.

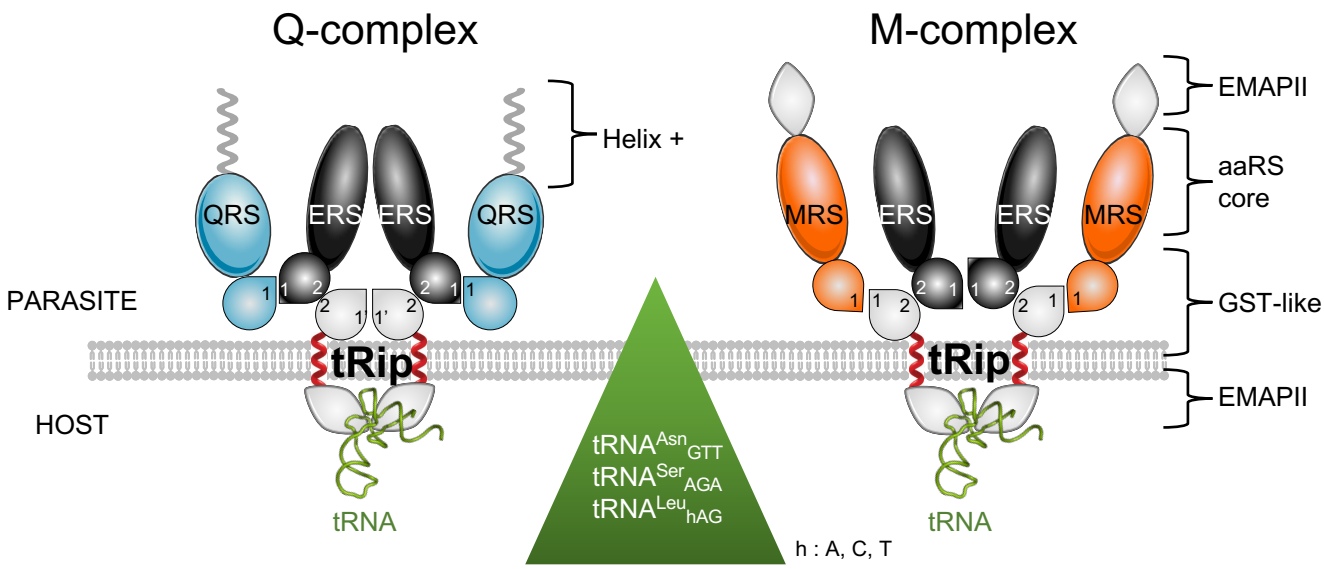
Q-complex
M-complex
Helix +
QRS
ERS
ERS
QRS
MRS
ERS
ERS
MRS
EMAPII
aaRS
core
GST-like
EMAPII
PARASITE
HOST
tRip
tRip
tRNA
tRNA
tRNA^Asn_GTT
tRNA^Ser_AGA
tRNA^Leu_hAG
h : A, C, T

Fig. 1

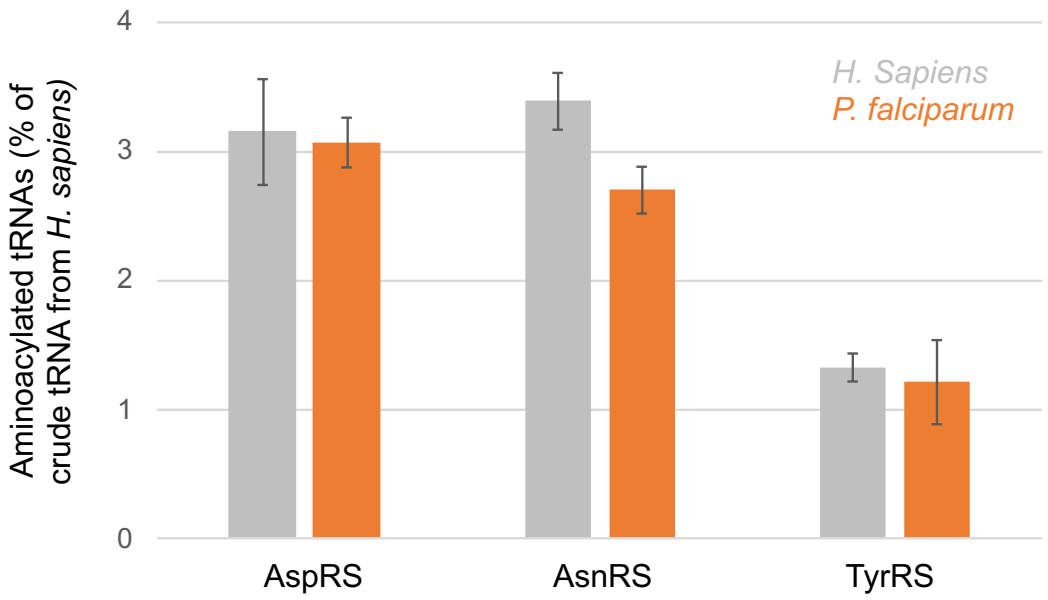
Aminoacylated tRNAs (% of crude tRNA from H. sapiens)
4
3
2
1
0
H. Sapiens
P. falciparum
AspRS
AsnRS
TyrRS

Fig. 2

a

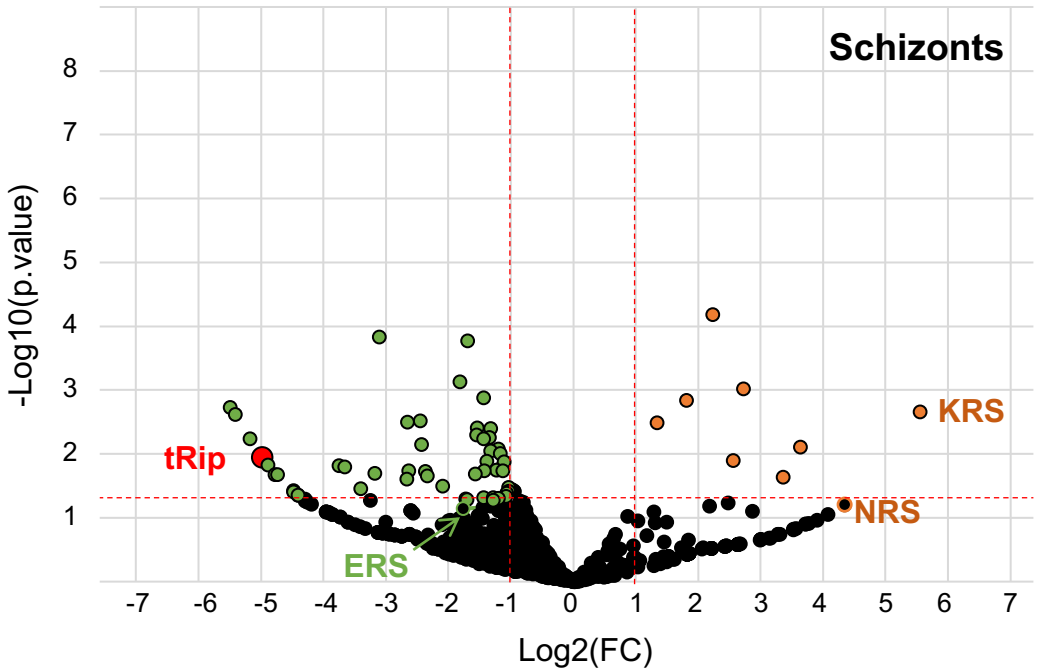
Schizonts
-Log10(p.value)
Log2(FC)
tRip
ERS
KRS
NRS

b

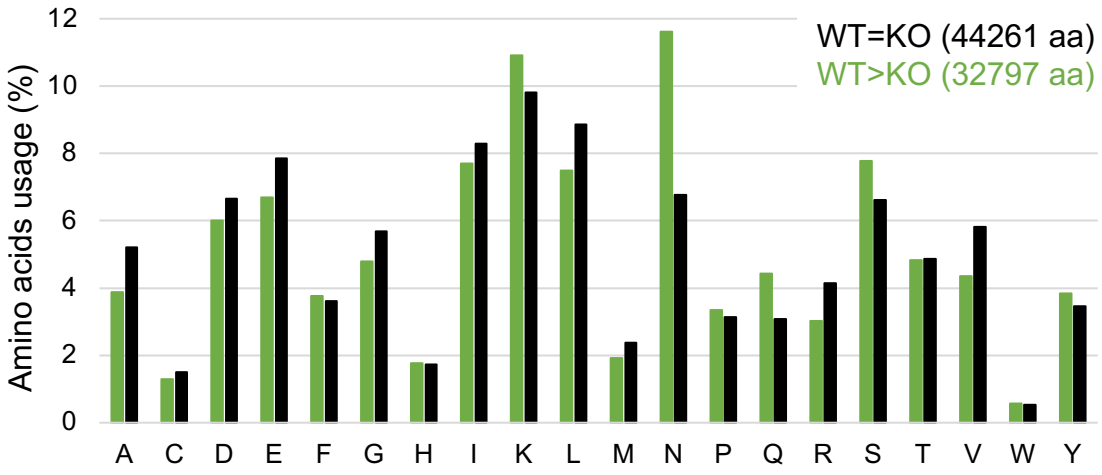
WT=KO (44261 aa)
WT>KO (32797 aa)
Amino acids usage (%)
A C D E F G H I K L M N P Q R S T V W Y

Fig. 3

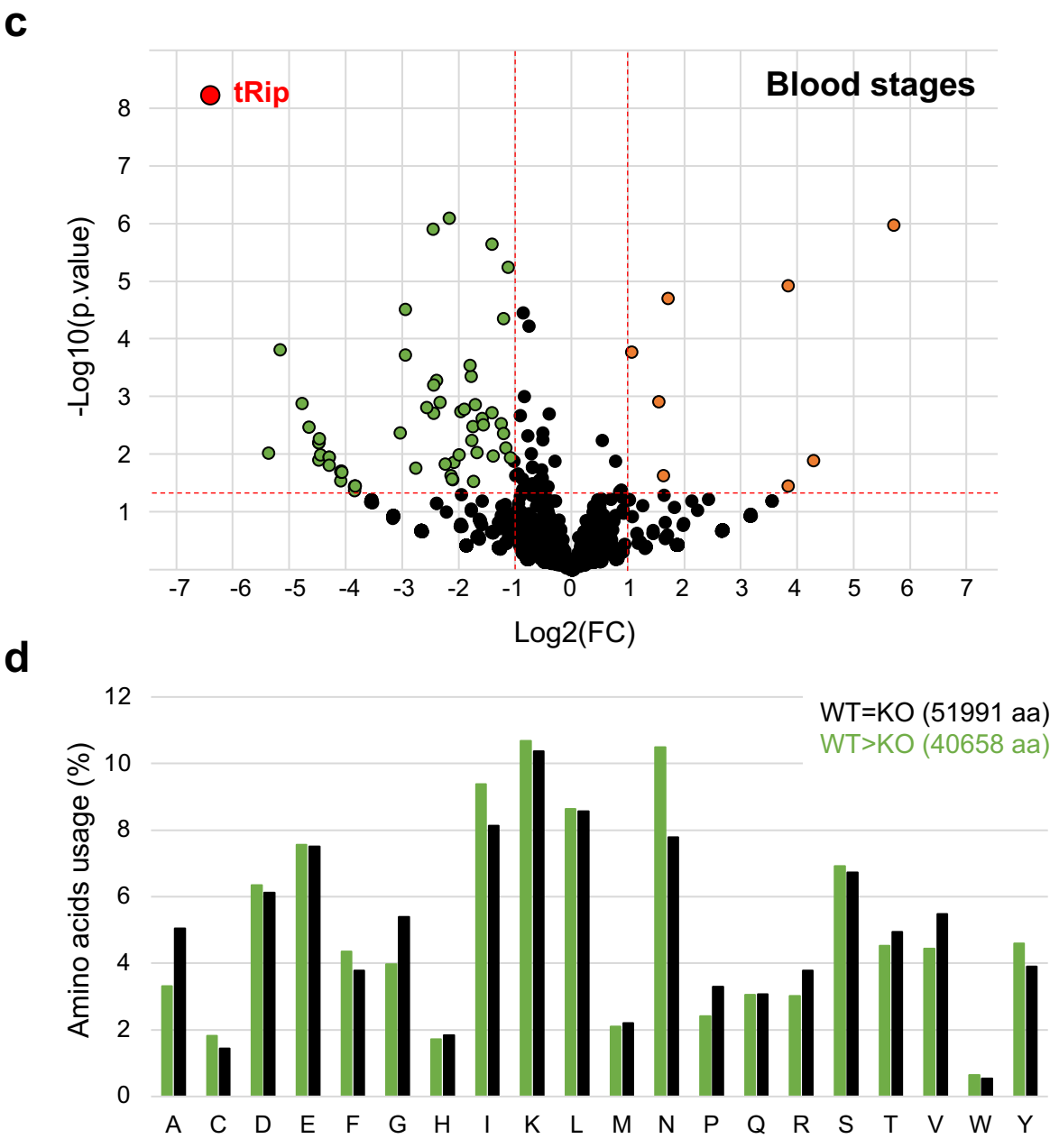
c
tRip
Blood stages
-Log10(p.value)
Log2(FC)
d
WT=KO (51991 aa)
WT>KO (40658 aa)
Amino acids usage (%)
A C D E F G H I K L M N P Q R S T V W Y

Fig. 3

P. falciparum

Protein id	Prot length	Asn (%)	function
PF3D7_0923500	357	42.017	cyclin-dependent kinases regulatory subunit
PF3D7_1366900	685	34.891	conserved protein. unknown function
PF3D7_0218200	807	33.333	SUZ domain-containing protein. putative
PF3D7_1439500	1074	32.961	oocyst rupture protein 2. putative
PF3D7_0706500	1706	32.298	conserved Plasmodium protein. unknown function
PF3D7_0811300	**1774**	**32.187**	**CCR4-associated factor 1**
PF3D7_0611800	3248	31.989	conserved Plasmodium protein. unknown function
PF3D7_1249700	908	31.608	conserved Plasmodium protein. unknown function
PF3D7_0817300	2235	31.588	conserved Plasmodium protein. unknown function
PF3D7_1236100	445	31.236	clustered-asparagine-rich protein
PF3D7_0525300	481	31.185	conserved protein. unknown function
PF3D7_0323800	977	31.116	conserved Plasmodium protein. unknown function
PF3D7_0212100	1844	31.074	conserved Plasmodium protein. unknown function
PF3D7_1329600	301	30.897	conserved Plasmodium protein. unknown function
PF3D7_1473500	675	30.667	conserved Plasmodium protein. unknown function
PF3D7_0926100	3178	30.585	protein kinase. putative
PF3D7_0411000	1570	30.382	AP2 domain transcription factor AP2-Z
PF3D7_1146800	3188	30.332	conserved Plasmodium protein. unknown function
PF3D7_1337500	3334	30.324	conserved Plasmodium protein. unknown function
PF3D7_1317200	2672	30.202	AP2 domain transcription factor AP2-FG
PF3D7_0602000	1437	29.923	zinc finger protein. putative
PF3D7_1222600	2432	29.852	AP2 domain transcription factor AP2-G
PF3D7_0906600	843	29.775	zinc finger protein. putative
PF3D7_1205500	1785	29.636	zinc finger protein. putative
PF3D7_0629400	**780**	**29.487**	**polyadenylate-binding protein 3. putative**
PF3D7_0304600	397	29.471	circumsporozoite (CS) protein

P. yoelii

Protein id	Prot length	Asn (%)	function
PY17X_1428300	**1807**	**30.825**	**CCR4-associated factor 1. putative**
PY17X_1129700	**535**	**30.654**	**polyadenylate-binding protein 3**
PY17X_0111700	2872	28.482	conserved Plasmodium protein. unknown function
PY17X_1225100	169	28.402	conserved Plasmodium protein. unknown function
PY17X_1213800	261	27.969	rhoptry associated adhesin. putative
PY17X_1341400	610	27.869	conserved Plasmodium protein. unknown function
PY17X_1334500	967	27.611	AP2 domain transcription factor AP2-SP. putative
PY17X_0929400	122	27.049	heat shock factor-binding protein 1
PY17X_1453200	411	26.764	clustered-asparagine-rich protein. putative
PY17X_1356400	1912	26.569	conserved Plasmodium protein. unknown function
PY17X_0309500	987	26.444	conserved Plasmodium protein. unknown function
PY17X_1307200	960	26.354	oocyst rupture protein 2. putative
PY17X_1110800	1966	26.144	KH domain-containing protein. putative
PY17X_0614700	1230	25.528	apicomplexan kinetochore protein 3. putative
PY17X_1313200	552	25.362	RNA-binding protein. putative
PY17X_1334300	2085	25.324	conserved Plasmodium protein. unknown function
PY17X_0103500	483	25.259	RNA-binding protein. putative
PY17X_1440000	2341	25.16	AP2 domain transcription factor AP2-G
PY17X_0806800	1567	25.144	conserved Plasmodium protein. unknown function
PY17X_0315400	830	25.06	SUZ domain-containing protein. putative
PY17X_1417400	2502	25.02	AP2 domain transcription factor AP2-SP. putative
PY17X_1403500	312	25	LisH domain-containing protein. putative
PY17X_0930400	329	24.924	conserved Plasmodium protein. unknown function
PY17X_1426800	201	24.876	U1 small nuclear ribonucleoprotein C. putative
PY17X_1454600	1693	24.867	conserved Plasmodium protein. unknown function
PY17X_1205700	1022	24.853	E3 ubiquitin-protein ligase. putative
PY17X_0903500	3240	24.846	sporozoite and liver stage asparagine-rich protein
PY17X_1457300	1863	24.745	RNA-binding protein. putative
PY17X_1465200	746	24.665	conserved Plasmodium protein. unknown function
PY17X_0943000	142	24.648	conserved Plasmodium protein. unknown function

P. berghei

Protein id	Prot length	Asn (%)	function
PBANKA_1426200	**1801**	**30.372**	**CCR4-associated factor 1**
PBANKA_0927400	122	28.689	heat shock factor-binding protein 1
PBANKA_0928400	358	28.492	conserved Plasmodium protein. unknown function
PBANKA_1128200	**511**	**27.984**	**polyadenylate-binding protein 3.**
PBANKA_1210600	256	27.734	rhoptry associated adhesin. putative
PBANKA_1303400	875	27.429	oocyst rupture protein 2
PBANKA_0612200	1251	27.338	apicomplexan kinetochore protein 3
PBANKA_0939600	3296	27.306	polyadenylate-binding protein-interacting protein 1
PBANKA_1336700	607	27.183	conserved Plasmodium protein. unknown function
PBANKA_1329600	2115	27.139	conserved Plasmodium protein. unknown function
PBANKA_1107200	677	27.031	protein CAF40. putative
PBANKA_1245900	412	26.942	Plasmodium exported protein. unknown function
PBANKA_0110100	2611	26.848	conserved Plasmodium protein. unknown function
PBANKA_1351300	1864	26.019	conserved Plasmodium protein. unknown function
PBANKA_0101900	478	25.941	RNA-binding protein. putative
PBANKA_1100600	54	25.926	PIR protein. pseudogene
PBANKA_1329800	943	25.875	AP2 domain transcription factor AP2-SP
PBANKA_0804100	1572	25.509	conserved Plasmodium protein. unknown function
PBANKA_0103300	2033	25.43	GYF domain-containing protein. putative
PBANKA_0308900	918	25.272	conserved Plasmodium protein. unknown function
PBANKA_1450700	397	25.189	clustered-asparagine-rich protein. putative
PBANKA_0604500	2264	25.044	high mobility group protein B3. putative
PBANKA_1415700	2487	24.568	AP2 domain transcription factor AP2-FG
PBANKA_1109700	1930	24.508	KH domain-containing protein. putative
PBANKA_0514300	947	24.498	conserved Plasmodium protein. unknown function

P. chabaudi

Protein id	Prot length	Asn (%)	function
PCHAS_1428000	**1775**	**29.972**	**CCR4-associated factor 1**
PCHAS_1341300	641	29.173	conserved Plasmodium protein. unknown function
PCHAS_0915900	329	28.875	conserved Plasmodium protein. unknown function
PCHAS_0916900	122	27.869	heat shock factor-binding protein 1. putative
PCHAS_1127700	**510**	**27.647**	**polyadenylate-binding protein 3**
PCHAS_1211300	246	26.423	rhoptry associated adhesin. putative
PCHAS_1306600	957	26.332	oocyst rupture protein 2. putative
PCHAS_0804400	1528	26.113	conserved Plasmodium protein. unknown function
PCHAS_0110700	2594	25.867	conserved Plasmodium protein
PCHAS_1426400	533	25.328	protein KIC7. putative
PCHAS_1453000	396	25.253	clustered-asparagine-rich protein. putative
PCHAS_0613900	1198	25.209	apicomplexan kinetochore protein 3. putative
PCHAS_1334400	984	24.695	AP2 domain transcription factor AP2-SP
PCHAS_1142300	556	24.46	conserved protein. unknown function
PCHAS_0311100	953	24.449	conserved Plasmodium protein. unknown function
PCHAS_0625600	336	24.405	fam-c protein
PCHAS_0514400	948	24.262	conserved Plasmodium protein. unknown function
PCHAS_1417500	2390	24.226	AP2 domain transcription factor AP2-FG
PCHAS_0703300	3131	24.082	sporozoite and liver stage asparagine-rich protein
PCHAS_1454400	1526	24.05	conserved Plasmodium protein. unknown function
PCHAS_0102600	488	23.975	RNA-binding protein. putative
PCHAS_1109400	1837	23.625	KH domain-containing protein
PCHAS_1464900	726	23.416	conserved Plasmodium protein. unknown function
PCHAS_0520100	1543	23.396	conserved Plasmodium protein
PCHAS_0413300	893	23.292	RING finger protein RNF1. putative
PCHAS_1457100	1728	23.09	RNA-binding protein. putative

P. knowlesi

Protein id	Prot length	Asn (%)	function
PKNH_0515300	239	23.013	apical asparagine-rich protein AARP
PKNH_API05400	97	21.649	hypothetical protein
PKNH_0934400	741	20.783	conserved Plasmodium protein. unknown function
PKNH_1427000	689	20.174	conserved protein. unknown function
PKNH_1245200	334	20.06	trailer hitch homolog. putative
PKNH_1236600	775	19.613	RNA-binding protein. putative
PKNH_1429400	**1971**	**19.533**	**CCR4-associated factor 1. putative**
PKNH_API04400	125	19.2	apicoplast ribosomal protein L11. putative
PKNH_0826500	1208	19.123	zinc finger protein. putative
PKNH_1427400	615	19.024	protein KIC7. putative
PKNH_1007500	471	18.684	conserved protein. unknown function
PKNH_0301400	75	18.667	RNA-binding protein. putative
PKNH_0812000	281	18.505	rhoptry associated adhesin. putative
PKNH_1430100	908	18.392	ATP-dependent RNA helicase DBP1. putative
PKNH_1215100	1094	18.282	AP2 domain transcription factor AP2-EXP. putative
PKNH_1007800	880	18.182	zinc finger protein. putative
PKNH_0101500	143	18.182	conserved Plasmodium protein. unknown function
PKNH_1455800	474	18.143	clustered-asparagine-rich protein. putative
PKNH_API02500	89	17.978	apicoplast ribosomal protein S19. putative
PKNH_1348500	497	17.706	CUGBP Elav-like family member 2. putative
PKNH_1264600	147	17.687	parasitophorous vacuolar protein 3. putative
PKNH_0811000	119	17.647	BET1-like protein. putative
PKNH_0917400	721	17.614	conserved Plasmodium protein. unknown function
PKNH_1120100	**644**	**17.547**	**polyadenylate-binding protein 3. putative**
PKNH_API03300	80	17.5	hypothetical protein
PKNH_API04900	103	17.476	hypothetical chloroplast reading frame 93. putative
PKNH_0827400	1201	17.402	RING finger protein RNF1. putative
PKNH_API05300	1021	17.042	DNA-directed RNA polymerase subunit beta. putative
PKNH_0621400	1861	17.034	conserved Plasmodium protein. unknown function

P. vivax

Protein id	Prot length	Asn (%)	function
PVP01_0937100	779	24.904	conserved Plasmodium protein. unknown function
PVP01_1001950	86	22.093	PIR protein. pseudogene
PVP01_API04400	97	21.649	hypothetical protein
PVP01_0531900	297	20.539	apical asparagine-rich protein AARP
PVP01_1426900	699	19.886	conserved protein. unknown function
PVP01_API01500	89	19.101	apicoplast ribosomal protein S19. putative
PVP01_1269800	341	19.062	trailer hitch homolog. putative
PVP01_API02300	80	18.75	hypothetical protein
PVP01_0421700	91	18.681	conserved protein. unknown function
PVP01_0811300	118	18.644	BET1-like protein. putative
PVP01_API03400	125	18.4	apicoplast ribosomal protein L11. putative
PVP01_API01200	202	18.317	50S ribosomal protein L4. putative
PVP01_1401600	205	18.049	Plasmodium exported protein. unknown function
PVP01_1218000	139	17.986	parasitophorous vacuolar protein 3. putative
PVP01_1429000	**2030**	**17.98**	**CCR4-associated factor 1. putative**
PVP01_0705100	842	17.815	zinc finger protein. putative
PVP01_API04100	975	17.744	DNA-directed RNA polymerase subunit beta''. putative
PVP01_1429700	923	17.66	ATP-dependent RNA helicase DBP1. putative
PVP01_API03900	121	17.355	hypothetical chloroplast reading frame 93. putative
PVP01_API04300	1021	17.336	DNA-directed RNA polymerase subunit beta. putative
PVP01_1404300	1063	17.31	LisH domain-containing protein. putative
PVP01_1339100	503	17.296	CUGBP Elav-like family member 2. putative
PVP01_1120100	**670**	**17.164**	**polyadenylate-binding protein 3. putative**
PVP01_0010790	112	16.964	PIR protein
PVP01_1427300	661	16.944	protein KIC7. putative
PVP01_0103500	143	16.783	conserved Plasmodium protein. unknown function
PVP01_API02500	132	16.667	apicoplast ribosomal protein S11. putative
PVP01_1001850	42	16.667	PIR protein. pseudogene
PVP01_1008800	1006	16.501	zinc finger protein. putative
PVP01_1420400	75	16	conserved protein. unknown function

Fig. 4

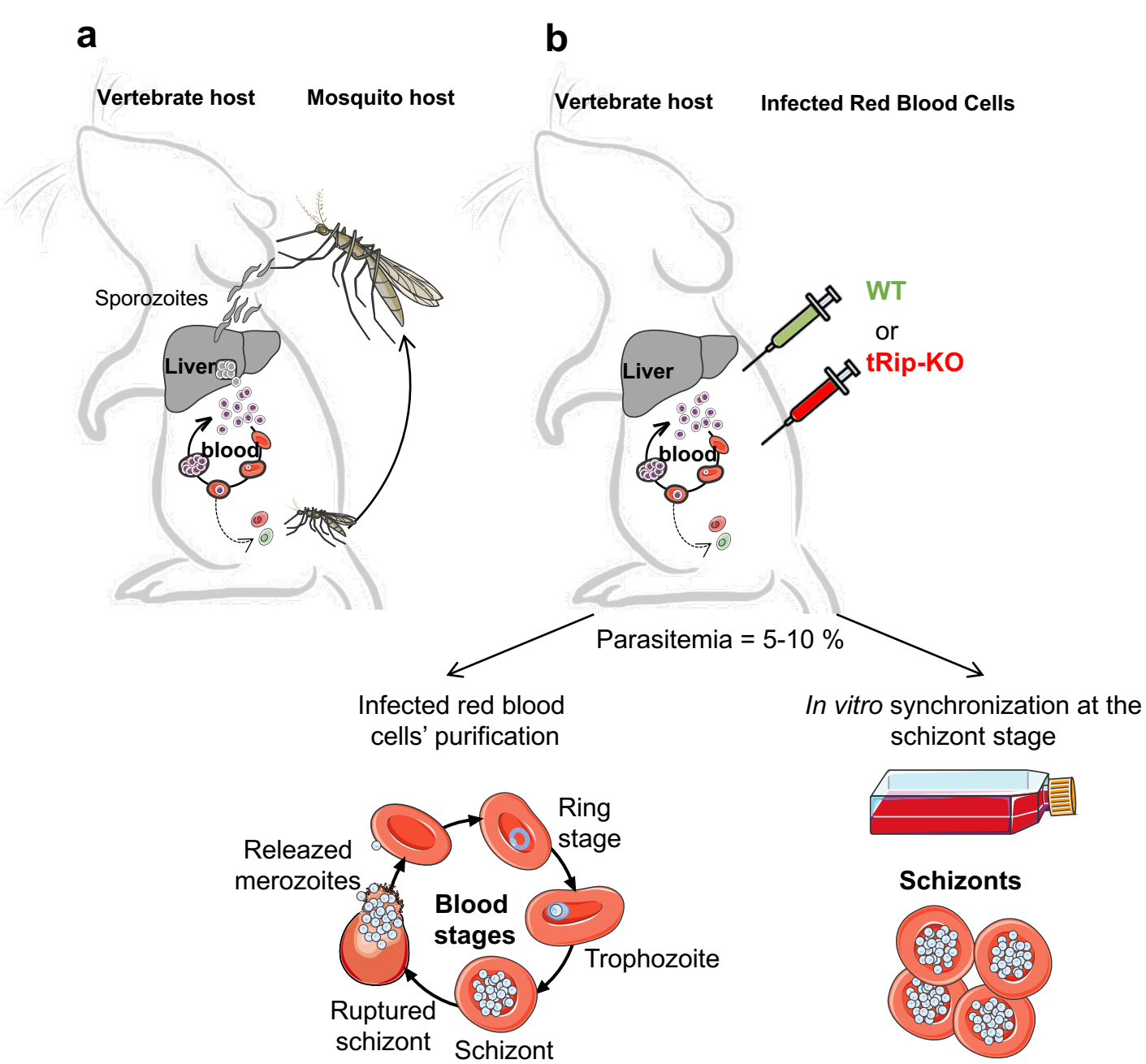

Supplementary Fig. S1. Mice infections and sample preparation. (**a**) *Plasmodium* life cycle. The cycle of vertebrate infection starts when a mosquito injects sporozoites into the host. Sporozoites invade hepatocytes (liver stage), multiply, and produce tens of thousands of merozoites per infected hepatocyte[1]. Merozoites exit the liver and develop in red blood cells (blood stages) to produce 10 to 30 new merozoites per intra-erythrocytic cycle[2]. Some of the erythrocytic merozoites differentiate into gametocytes (sexual forms, dashed lines)[3]. Fertilization takes place in mosquitoes where gametocytes are ingested during a blood meal. In 8-15 days, sporozoites invade the mosquito salivary glands, completing the cycle. (**b**) Alternatively, mice are infected with frozen stocks of red blood cells infected with wild-type (GFP) or tRip-KO (mCherry) *P. berghei* parasites. Three to six days later (5-10% parasitemia), infected blood is collected and used as is for analysis (all blood stages) or synchronized *in vitro* to the schizont stage[4]. "All blood stages" samples contain rings, trophozoites and merozoites.

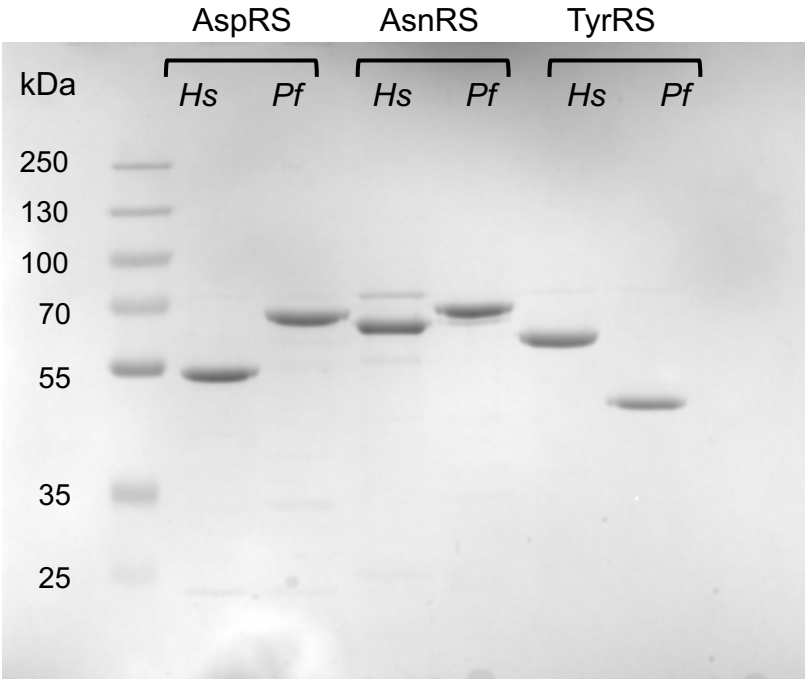

Supplementary Fig. S2. Gel analysis of aminoacyl-tRNA synthetases. One µg of each recombinant enzyme aspartyl- (DRS), asparaginyl- (NRS) and tyrosyl-(YRS) tRNA synthetases from *H. sapiens* (*Hs*) or *P. falciparum* (*Pf*) was run on a 10 % SDS PAGE.

a

Average Ct (triplicate)					ΔCt			Efficiency			Mean	RQ	Mean RQ	SD	SEM
Genotype	Sample	MCM7	Hsp70	EF1-α	MCM7	Hsp70	EF1-α	MCM7	Hsp70	EF1-α	Hsp70/EF1-α	MCM7	MCM7		
WT	2	19,82	19,77	17,86	-1,10	-0,59	0,88	2,14	1,50	0,54	0,90	2,37			
WT	3	20,73	21,54	16,21	-0,19	1,18	-0,77	1,14	0,44	1,71	0,87	1,32	**1,77**	0,49	**0,28**
WT	4	20,79	20,96	17,50	-0,13	0,60	0,52	1,09	0,66	0,70	0,68	1,62			
KO	1	21,87	19,99	16,73	0,95	-0,37	-0,25	0,52	1,29	1,19	1,24	0,42			
KO	2	21,27	19,75	16,30	0,35	-0,61	-0,68	0,78	1,52	1,60	1,56	0,50	**0,62**	0,25	**0,14**
KO	4	21,04	20,14	17,27	0,12	-0,22	0,29	0,92	1,16	0,82	0,97	0,94			
Mean		20,92	20,36	16,98									p-value = 0,03		

Average Ct (triplicate)					ΔCt			Efficiency			Mean	RQ	Mean RQ	SD	SEM
Genotype	Sample	ChAF1C	Hsp70	EF1-α	ChAF1C	Hsp70	EF1-α	ChAF1C	Hsp70	EF1-α	Hsp70/EF1-α	ChAF1C	ChAF1C		
WT	2	17,89	19,37	15,75	-3,29	-2,68	-2,32	9,75	6,42	4,98	5,65	1,72			
WT	3	24,23	26,49	23,51	3,06	4,44	5,45	0,12	0,05	0,02	0,03	3,70	**2,70**	0,88	**0,51**
WT	4	21,34	23,53	19,75	0,16	1,48	1,69	0,89	0,36	0,31	0,33	2,67			
KO	1	23,80	23,57	16,11	2,63	1,52	-1,96	0,16	0,35	3,88	1,16	0,14			
KO	2	19,23	18,95	15,72	-1,95	-3,10	-2,35	3,85	8,59	5,08	6,61	0,58	**0,48**	0,27	**0,15**
KO	4	20,56	20,41	17,55	-0,82	-1,64	-0,52	1,53	3,12	1,43	2,11	0,72			
Mean		21,18	22,05	18,07									p-value = 0,02		

Average Ct (triplicate)					ΔCt			Efficiency			Mean	RQ	Mean RQ	SD	SEM
Genotype	Sample	UF	Hsp70	EF1-α	UF	Hsp70	EF1-α	UF	Hsp70	EF1-α	Hsp70/EF1-α	UF	UF		
WT	2	19,91	19,78	16,19	-2,09	-0,61	-0,72	4,26	1,53	1,64	1,59	2,68			
WT	3	21,13	21,74	17,98	-0,87	1,35	1,07	1,83	0,39	0,48	0,43	4,23	**3,23**	0,77	**0,44**
WT	4	20,98	20,92	17,30	-1,02	0,53	0,39	2,03	0,69	0,76	0,73	2,79			
KO	1	24,04	19,92	16,70	2,04	-0,47	-0,21	0,24	1,39	1,15	1,27	0,19			
KO	2	22,68	19,47	16,01	0,68	-0,93	-0,90	0,62	1,90	1,86	1,88	0,33	**0,34**	0,14	**0,08**
KO	4	23,26	20,54	17,26	1,26	0,15	0,35	0,42	0,90	0,78	0,84	0,50			
Mean		22,00	20,40	16,91									p-value = 0,0046		

Gene ID and name (expression status in tRip-KO)	Primers		Primer efficiency	r^2
PBANKA_0803100 DNA replication licensing factor MCM7 (down regulated)	Forward Reverse	CAACCATTTCCCCTGAACTA CACTATCTCTTACCCTTGCC this study	105.4 %	0.965
PBANKA_0203000 chromatin assembly 1 (down regulated)	Forward Reverse	GGACATTTTGCATCTGGAAG GCATCTAACTCTTCACCGAT this study	99.8 %	0,98
PBANKA_1029400 unknown function (down regulated)	Forward Reverse	TAGCTACTTGTTTACCGCAA TGAGGCCCCTTTAATTACTCTGT this study	96.0%	0.990
Reference genes				
PBANKA_1133300 EF1-α	Forward Reverse	TGGAACCACCCAAAAGACCA ACAACAGCAGATGGAGCGAA Tokunaga et al., 2019	100.7%	1
PBANKA_0914400 Hsp70	Forward Reverse	AGAGAAGCAGCTGAAACAGC TCCCTTTAATAAATCATGGC Sanyal et al., 2013	106.9%	0.999

RNA analyses

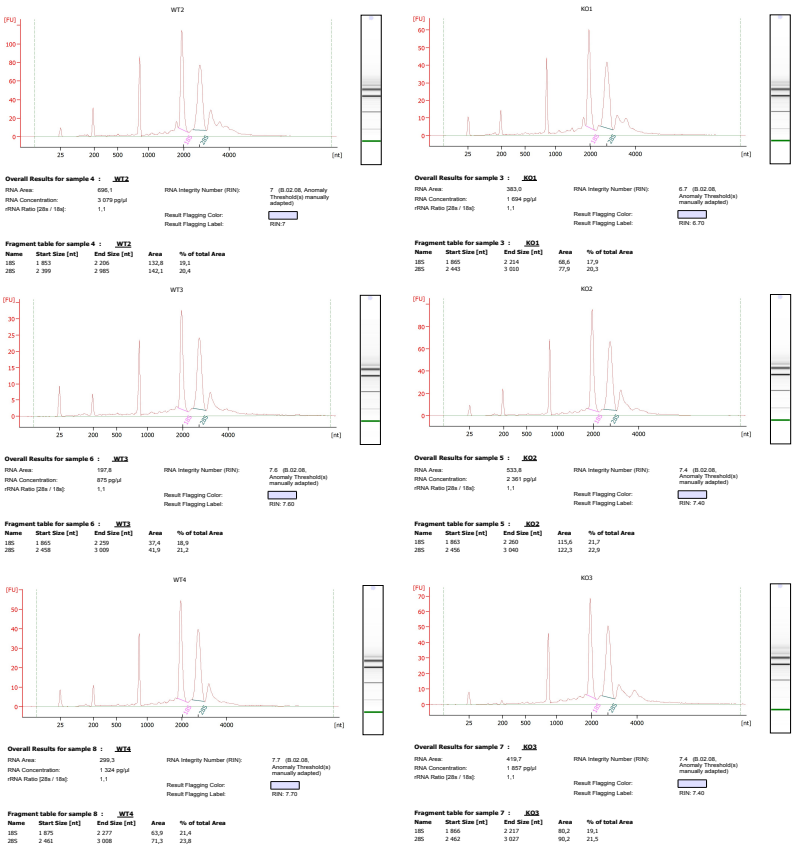

b

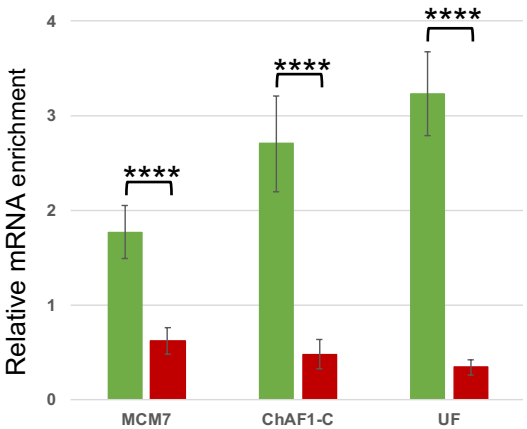

Supplementary Fig. S3. qRT-PCR analysis of the mRNAs coding for deregulated proteins in the tRip-KO parasite. The relative enrichment of mRNA was measured by qRT-PCR and determined by the ΔΔ*Ct* method using both EF1-a (PBANKA_1133300) and Hsp70 (PBANKA_0914400) as normalizers. mRNAs are coding for down-regulated proteins: the DNA replication licensing factor MCM7 (MCM7, FC = 5.7, *p-value* =1.3 x 10^{-6}), chromatin assembly factor 1-subunit C (ChAF1-C, FC = 2.2, *p-value* = 5.7 x 10^{-6}) and a protein with unknown function (UF, FC = 3.6, *p-value* = 2.9 x 10^{-4}). (**a**) QRT-PCR raw data. For each "all blood stages" samples, qRT-PCR data the primers as well as the quality control of the RNA samples are shown. (**b**) Error bars represent the standard errors of the means (SEM) of three independent experiments performed on "All blood stages" samples, each corresponding to triplicate qRT-PCR measurements (S4 Table). Asterisks indicate statistically significant differences with the WT control mRNA: **** *p-value* < 0.0001 based on Student's *t* test.

a

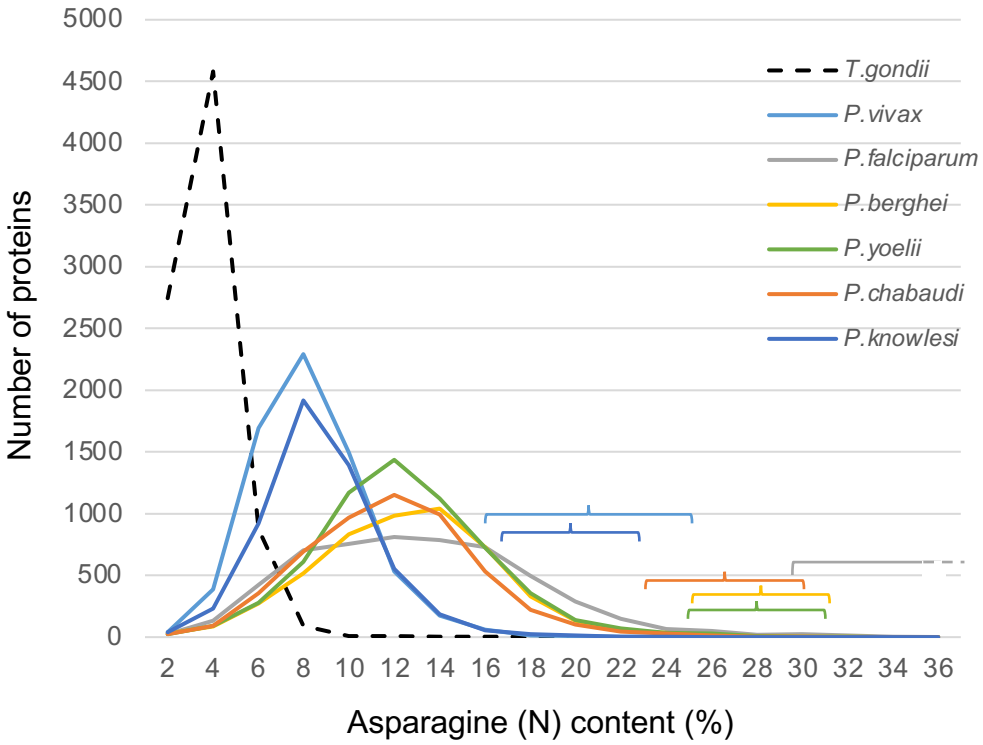

b

CAF-1 (*P. falciparum*)
AF-C0H4T9

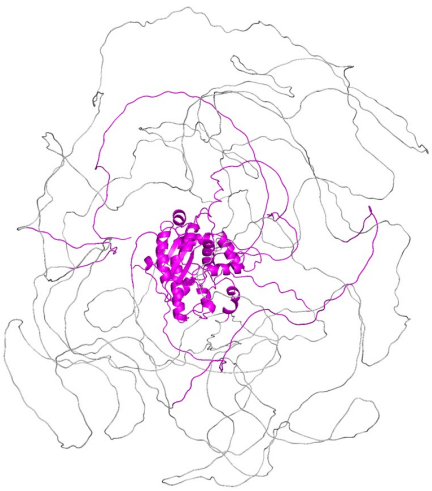

PABP-3 (*P. falciparum*)
AF-C6KTC9

c

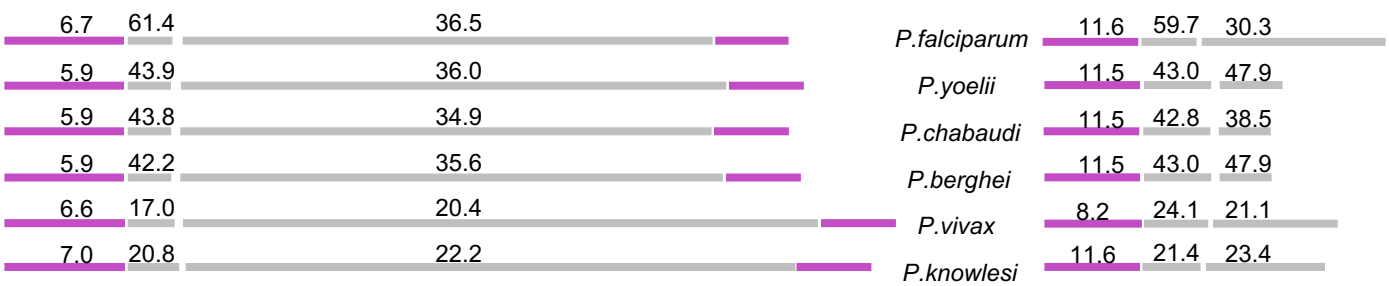

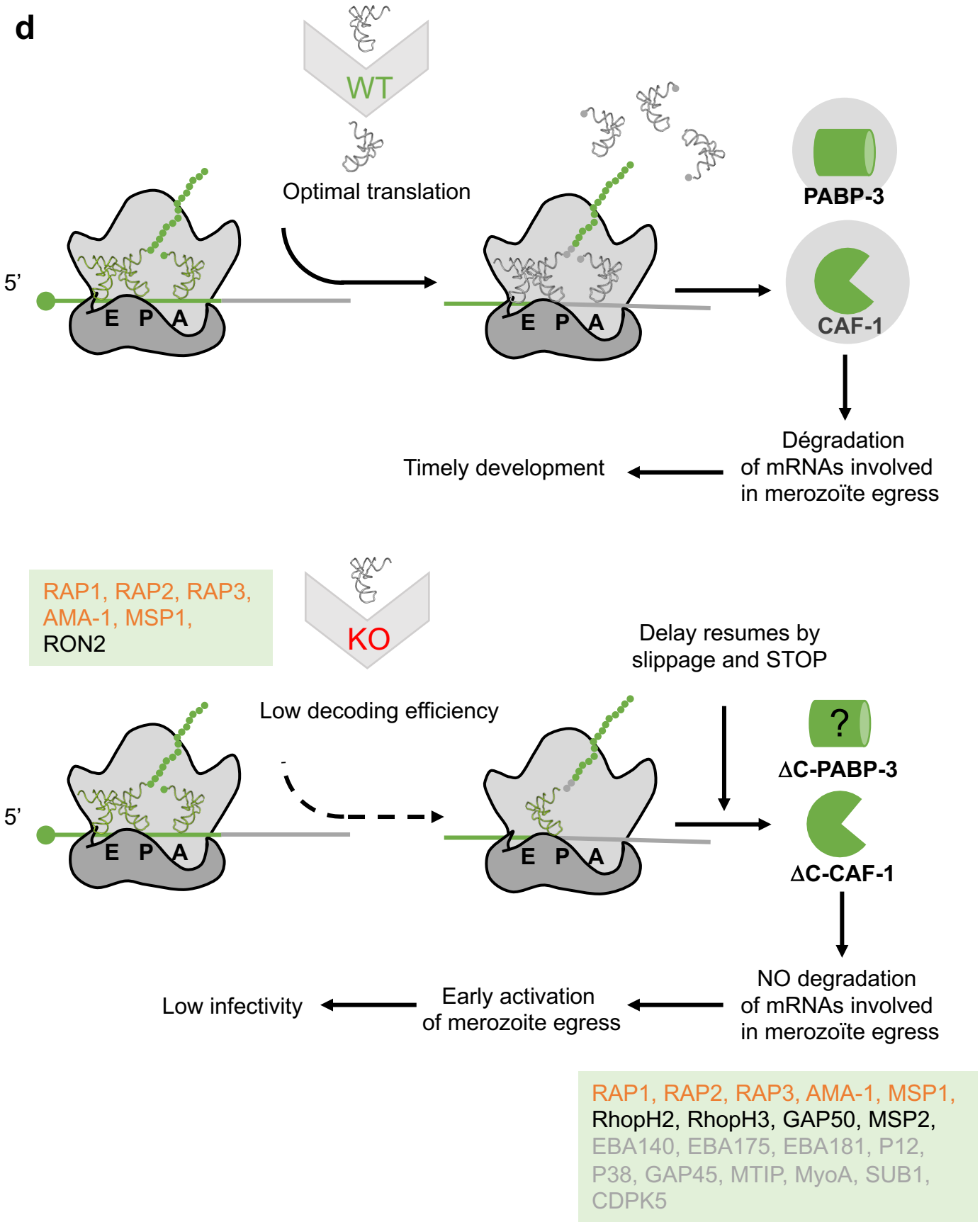
d
WT
Optimal translation
5'
E P A
E P A
PABP-3
CAF-1
Dégradation
of mRNAs involved
in merozoïte egress
Timely development
RAP1, RAP2, RAP3,
AMA-1, MSP1,
RON2
KO
Delay resumes by
slippage and STOP
Low decoding efficiency
5'
E P A
E P A
?
ΔC-PABP-3
ΔC-CAF-1
NO degradation
of mRNAs involved
in merozoïte egress
Early activation
of merozoite egress
Low infectivity
RAP1, RAP2, RAP3, AMA-1, MSP1,
RhopH2, RhopH3, GAP50, MSP2,
EBA140, EBA175, EBA181, P12,
P38, GAP45, MTIP, MyoA, SUB1,
CDPK5

Supplementary Fig. S4. Asparagine frequency in *Plasmodium* proteins and functional link between tRip and CAF-1. (**a**) Proteomes of *P. falciparum, P. yoelii, P. berghei, P. chabaudi*, *P. knowlesi* and *P. vivax* were compared and the proteome of *Toxoplasma gondii* was used as a negative control[5]. For each species, the number of proteins is indicated for a given asparagine content. Brackets show the top 0.5 % proteins containing the highest percentage of asparagine residues. (**b**) AlphaFold models of *P. falciparum* CAF-1 and PABP-3 (10). Both models show conserved domains (pink) and an unfolded asparagine-rich *Plasmodium* specific C-terminal extensions (grey). (**c**) Domain alignments of CAF-1 and PABP-3. The corresponding domains are shown with the same color code and the corresponding percentage of asparagine. (**d**) In WT parasites, the asparagine-rich C-terminal domains of *Plasmodium* CAF-1 and PABP-3 are efficiently translated thanks to $tRNA^{Asn}$ provided by tRip-mediated tRNA import from the host. Full-length CAF-1 can thus down-regulate specific mRNAs including those involved in egress and invasion that adequately control parasite development. On the contrary, in the tRip-KO parasite, translation of the C-terminal domains of CAF-1 and PABP-3 is hindered by the absence of host $tRNA^{Asn}$. The delay in translation can lead to frameshifting and the occurrence of stop codons. The resulting DC-CAF-1 protein can no longer regulate the translation of genes involved in parasite egress/invasion leading to early release of infectivity-deficient immature merozoites. Genes up-regulated in both mutants are highlighted in orange, they correspond to roptry-associated proteins 1, 2 and 3 (RAP1, PF3D7_1410400/PBANKA_1032100; RAP2/3, PF3D7_0501600/0501500, PBANKA_1101400), apical membrane antigen (AMA1, PF3D7_1133400/PBANKA_0915000) and merozoite surface protein 1 (MSP1, PF3D7_0930300/PBANKA_0831000). Up-regulated genes involved in merozoite's egress either in *P. falciparum* ΔC-CAF1 mutant or *P. berghei* tRip-KO parasite are listed inside green boxes: genes not in common between both strains are indicated in black: merozoite surface protein 2 (MSP2, PF3D7_0206800), glidosome associated protein 50 (GAP50, PF3D7_0918000/PBANKA_0819000), high molecular weight rhoptry proteins 2 and 3 (RhopH2, PF3D7_0929400/PBANKA_0830200 and RhopH3, PF3D7_0905400/PBANKA0416000) and Rhoptry neck protein 2 (RON2, PBANKA_1315700); Ten genes were up-regulated in the ΔC-CAF-1 mutant but were not detectable in blood stages proteomes. They correspond to: erythrocyte binding antigens 140, 175 and 181 (EBA140, PF3D7_1301600; EBA175, PF3D7_0731500; EBA181, PF3D7_0102500), 6-cysteine proteins P12 and P38 (PF3D7_0612700 and PF3D7_0508000), glideosome-associated protein 45 (GAP45, PF3D7_1222700), myosin A-tail interaction protein (MTIP, PF3D7_1246400/PBANKA_1459500), myosin A (MyoA, PF3D7_1342600), subtilisin-like protease 1 (SUB1, PF3D7_0507500) and calcium-dependent protein kinase 5 (CDPK5, PF3D7_1337800).

References for supplementary figures

1. Rankin, K. E., Graewe, S., Heussler, V. T. & Stanway, R. R. Imaging liver-stage malaria parasites. *Cellular Microbiology* **12**, 569–579 (2010).
2. Cowman, A. F., Tonkin, C. J., Tham, W.-H. & Duraisingh, M. T. The Molecular Basis of Erythrocyte Invasion by Malaria Parasites. *Cell Host & Microbe* **22**, 232–245 (2017).
3. Talman, A. M., Clain, J., Duval, R., Ménard, R. & Ariey, F. Artemisinin Bioactivity and Resistance in Malaria Parasites. *Trends in Parasitology* **35**, 953–963 (2019).
4. Ramakrishnan, C. *et al.* Laboratory Maintenance of Rodent Malaria Parasites. in *Malaria* (ed. Ménard, R.) vol. 923 51–72 (Humana Press, 2012).
5. Amos, B. *et al.* VEuPathDB: the eukaryotic pathogen, vector and host bioinformatics resource center. *Nucleic Acids Research* **50**, D898–D911 (2022).